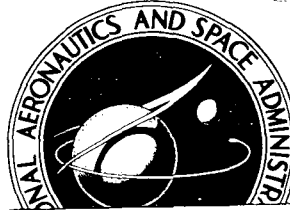


9/16 p

**NASA TECHNICAL  
MEMORANDUM**



AL

**NASA TM X-918**

(NASA-TM-X-918) AERODYNAMIC  
CHARACTERISTICS OF SEVERAL LIFTING AND  
NONLIFTING CONFIGURATIONS AT HYPERSONIC  
SPEEDS IN AIR AND HELIUM J.P. Arrington,  
et al (NASA) Jun. 1964 40 p

N72-73341

Unclas  
00/99 32182

X64 14731

Code 2

cat 03

NASA TM X-918

CONFIDENTIAL  
UNCLASSIFIED

TD-72-235 6-8-72

**AERODYNAMIC CHARACTERISTICS OF  
SEVERAL LIFTING AND NONLIFTING  
CONFIGURATIONS AT HYPERSONIC  
SPEEDS IN AIR AND HELIUM (U)**

*by James P. Arrington and Dal V. Maddalon  
Langley Research Center  
Langley Station, Hampton, Va.*

TECHNICAL MEMORANDUM X-918

AERODYNAMIC CHARACTERISTICS OF SEVERAL  
LIFTING AND NONLIFTING CONFIGURATIONS AT HYPERSONIC SPEEDS  
IN AIR AND HELIUM

By James P. Arrington and Dal V. Maddalon

Langley Research Center  
Langley Station, Hampton, Va.

GROUP 3  
Downgraded at 12-year  
intervals; not automatically  
declassified

~~ALL INFORMATION CONTAINED HEREIN IS UNCLASSIFIED~~  
~~This information contains information affecting the~~  
~~national defense of the United States within the~~  
~~meaning of the espionage laws, Title 18, U.S.C.,~~  
~~Secs. 793 and 794, the transmission or revelation~~  
~~of its contents in any manner to an unauthorized person~~  
~~is prohibited by law.~~

NATIONAL AERONAUTICS AND SPACE ADMINISTRATION

AERODYNAMIC CHARACTERISTICS OF SEVERAL  
LIFTING AND NONLIFTING CONFIGURATIONS AT HYPERSONIC SPEEDS  
IN AIR AND HELIUM\*

By James P. Arrington and Dal V. Maddalon

SUMMARY

14731

The longitudinal aerodynamic characteristics of several lifting and non-lifting configurations have been obtained in helium at a Mach number of 20.5 in a contoured nozzle and at a Mach number of about 24 in a conical nozzle. The helium results were compared with available air data for a Mach number range of 15 to 22. In addition, two hypersonic lifting configurations were tested in both conical and contoured nozzles in helium to determine the effects of source flow on aerodynamic forces and moments.

No appreciable effects of using helium as a test medium were noted in the normal-force coefficients, pitching-moment coefficients, or longitudinal stability characteristics in the angle-of-attack range of the tests. Essentially, all the differences in axial-force coefficients and consequently in drag coefficients can be attributed to the differences in Reynolds numbers of the tests rather than to the effect of the differences in specific-heat ratios of the gases. Therefore, within the scope of this investigation, the use of helium as a test medium for aerodynamic investigations appears to be satisfactory at high Mach numbers and ideal-gas conditions.

A comparison of force and moment data obtained in conical and contoured nozzles for one hypersonic lifting configuration indicated appreciable source flow effects which varied with model length. The data obtained on the second lifting configuration indicated small source flow effects which may be due at least in part to the position of the model in the flow field.

*author*

INTRODUCTION

Helium has become an established test medium for ideal-gas research in fluid mechanics at high Mach numbers. (See, for example, refs. 1 to 11.) In recent years, in addition to its primary role in fluid mechanics studies, the helium tunnel has been used for configuration studies in the field of aerodynamics. As more data have become available for comparison purposes, the

---

\*Title, Unclassified.

resulting problems of transforming helium data to equivalent air data have been of some concern. (See refs. 11 to 15.) The air-helium simulation problem at hypersonic speeds was examined analytically in references 13 and 15 for simple aerodynamic shapes which could be considered as isolated components of complete configurations.

The purpose of this paper is to compare the measured aerodynamic characteristics of several lifting and nonlifting configurations at approximately the same Mach number in air and helium. Force and moment studies were, in general, conducted at angles of attack from  $-5^\circ$  to  $20^\circ$  in the Langley 22-inch helium tunnel at Mach numbers of about 20 and 24. The helium data are compared with available data obtained in hotshot tunnels at a Mach number range of 15 to 22. Preliminary results of a portion of this air-helium study have been presented in reference 12.

In addition, this paper compares aerodynamic characteristics obtained in conical and contoured nozzles for two hypersonic lifting configurations. Longitudinal forces and moments were obtained at angles of attack from  $-5^\circ$  to  $20^\circ$  in the Langley 22-inch helium tunnel at a Mach number of about 24 in a conical nozzle and 20.5 in a contoured nozzle.

It should be noted that all experimental results contained in this paper are for essentially ideal-gas conditions, including data from hotshot facilities.

#### SYMBOLS

b	span, in.
$\bar{c}$	mean aerodynamic chord, in.
$C_A$	axial-force coefficient, $\frac{\text{Total axial force}}{qS}$
$C_D$	drag coefficient, $C_A \cos \alpha + C_N \sin \alpha$
$C_L$	lift coefficient, $C_N \cos \alpha - C_A \sin \alpha$
$C_m$	pitching-moment coefficient, $\frac{\text{Pitching moment}}{qS\bar{c}}$ or $\frac{\text{Pitching moment}}{qSl}$
$C_N$	normal-force coefficient, $\frac{\text{Normal force}}{qS}$
d	body diameter, in.
l	reference length, in.
L/D	lift-drag ratio

M	free-stream Mach number (at model nose in conical nozzle)
q	dynamic pressure, lb/sq in.
R	Reynolds number (subscript denotes reference length)
r	radius
S	reference area, sq in.
$x_{cp}$	center-of-pressure location, in.
$\alpha$	angle of attack, deg
$\gamma$	ratio of specific heats
$\epsilon$	angle of downwash, deg
$\sigma$	angle of sidewash, deg

Subscripts:

$\bar{c}$	mean aerodynamic chord, in.
i	inviscid value
N <sub>2</sub>	nitrogen gas
v	viscous value
l	reference length

## APPARATUS

### Wind Tunnel

The tests were conducted in the Langley 22-inch helium tunnel described in reference 11 at a Mach number of about 24 in a 5° half-angle conical nozzle. The flow produced by this nozzle has a Mach number gradient of about 0.08 per inch in the calibrated region. Additional tests were made at a Mach number of 20.5 in a contoured nozzle recently installed in this facility. A sketch of the tunnel with the contoured nozzle and test section is shown in figure 1.

The lateral-cross-section Mach number distributions in the test core of the flow in the contoured and conical nozzles for a stagnation pressure of 1,000 pounds per square inch gage are presented in figures 2(a) and 2(b), respectively. The deviations from the average Mach number within the core at three longitudinal locations in the test section are shown. The Mach numbers were determined from pitot pressure ratios which were corrected for real-gas

effects according to the method presented in reference 16. The accuracy of the Mach numbers is approximately  $\pm 0.2$ .

The flow angularity at three longitudinal stations in the  $M = 20$  contoured nozzle is presented in figure 3(a) for a stagnation pressure of 1,000 pounds per square inch gage. The position and the sign of the values indicate the direction of the flow (that is, left or right of a point indicates positive or negative sidewash, respectively, and above or below indicates positive or negative downwash, respectively). Within the accuracy of the measurements, which was about  $\pm 0.2^\circ$ , the flow angularity in the contoured nozzle appears to be negligible.

The flow angularity was determined by measuring the pressure differential between two pairs of diametrically opposed orifices on a  $40^\circ$  half-angle cone. The flow angles were obtained from a chart given in reference 17 which presents the flow angles in the plane of the diametrically opposed orifices as a function of the measured differential pressure coefficient.

In a similar manner the flow angularity in the  $5^\circ$  half-angle conical nozzle is presented in figure 3(b). Although this survey was made with a throat which gave a test Mach number of 27 instead of a Mach number of 24 which was used for this paper, the results are presented to give an indication of the type of flow angularity which develops in the test section of this nozzle.

### Models

Two groups of models were tested in this program: conical bodies and lifting winged configurations. These particular models were chosen because they had been previously tested in hotshot and shock tunnels at Mach numbers similar to the ones obtainable in the Langley 22-inch helium tunnel and the data were available for comparison purposes.

The  $10^\circ$  half-angle pointed cone and the slender conical configuration are described in figures 4(a) and 4(b), respectively. The winged ellipsoid configuration (see fig. 4(c)) is basically half of an ellipsoid modified by the addition of small wings, an inclined nose section, and by the removal of a small portion of the body at the lower aft end.

The winged reentry capsule shown in figure 4(d) is a possible escape capsule for a proposed winged reentry configuration. As can be seen from figure 4(d), the bottom surface of the model is inclined at an angle of  $4^\circ$  with respect to the longitudinal axis.

Drawings showing the dimensions of a winged reentry glide vehicle are presented in figure 4(e). Two models having scale factors of 0.016 and 0.0305 were tested. The configuration is basically a cone-cylinder body on a  $73^\circ$  sweptback slab wing. As indicated in the figure, the lower surface of the wing is flat except for the forward portion which has a fixed nose incidence of  $4^\circ$ .

## TESTS

All tests were conducted at a stagnation pressure automatically regulated at 1,000 pounds per square inch gage. Stagnation temperatures diminished rapidly from a high of about 120° F down to about 70° F during the course of each test as a result of decreasing reservoir pressure; an average of 75° F was chosen to be representative. The Mach number for tests conducted in the conical nozzle was chosen to be the average core Mach number at the nose of each model.

The tests were made with the use of several sting-supported internal strain-gage balances. During a particular test, a hydraulically actuated sting mechanism supporting the model-balance assembly continuously traversed through the angle-of-attack range at a rate generally not exceeding 3° per second. Specific angles of attack of the models were measured optically by the use of a light beam reflected onto a steel plate from a lens-prism assembly mounted on the models. Small photoelectric cells were attached to the plate at calibrated intervals. As the reflected light swept past each cell, an electrical relay was energized and caused a high-speed digital recorder to sample and record the strain-gage balance outputs on magnetic tape.

Because of the physical size of the photoelectric cells, small differences in the data at a given angle of attack were obtained depending on the direction from which the reflected light approached the cells. Since the photoelectric cells were approached from opposite directions during each test, two sets of data were obtained at each angle of attack as in reference 11. The difference between the two sets of data was found to be small and generally within the accuracy of the instrumentation. The results to be presented in this paper represent the average of the two sets of data. No base-pressure corrections were made to the data.

## RESULTS AND DISCUSSION

### Air-Helium Simulation

Basic aerodynamic data about the body axis of the models in both air and helium are presented as functions of angle of attack in figures 5 to 9. In addition, the basic data of the slender conical configuration and winged vehicles have been referenced to the wind-axis system in figures 6 to 8 for a comparison with the reference air data.

Both the air and helium data were obtained in tunnels by using the same type of nozzle (conical or contoured) for each configuration. The type of nozzle used is noted on each figure.

Figure 5 presents normal-force, axial-force, and pitching-moment coefficients for the sharp 10° cone at  $M = 19$  in nitrogen (unpublished test data obtained in the Von Karman facility of Arnold Engineering Development Center; designated AEDC hotshot) and at  $M = 24.3$  in helium (designated LRC helium).

The agreement between the hotshot and helium results is very good with the exception of the axial-force coefficients.

The results of the theoretical prediction presented in figure 5 indicate that the large difference in the axial-force results may be attributed to the difference in Reynolds number of the two tests. Estimated values of the axial-force coefficients due to skin friction were added to the theoretical pressure drag (induced pressure and base pressure effects being neglected) for both nitrogen and helium at zero angle of attack. (See fig. 5.) The skin friction was determined by applying the  $T'$  method given by Monaghan in reference 18 and by assuming no heat transfer for the helium data and a wall temperature of  $75^{\circ}\text{F}$  and a stagnation temperature of  $5,800^{\circ}\text{F}$  for the hotshot data.

Inviscid flow calculations presented in reference 12 indicate that at hypersonic Mach numbers, the Mach number as well as the specific heat ratio has an insignificant effect on cone axial force. In addition, the theory of reference 19 predicts negligible effects of  $M$  and  $\gamma$  on axial force as well as on normal force for cones having half-angles of  $20^{\circ}$  or less at hypersonic speeds. This prediction was verified experimentally in reference 20.

The aerodynamic characteristics of the slender conical configuration at  $M = 15.5$  in air and  $M = 20.5$  in helium are presented in figure 6. The unpublished air results were obtained in the Cornell Aeronautical Laboratory 48-inch shock tunnel (designated CALSH tunnel in figure). The basic air and helium data and the subsequent longitudinal stability parameters are in good agreement. The differences in the axial-force coefficient and consequently the drag coefficient may again be attributed to Reynolds number effects as previously shown for the  $10^{\circ}$  cone. The lower values of the drag coefficient obtained in helium results, of course, in a higher maximum  $L/D$ .

The aerodynamic characteristics of the winged ellipsoid at a Mach number of 16.5 and a Reynolds number of  $0.18 \times 10^6$  in air and at a Mach number of 24.3 and a Reynolds number of  $1.64 \times 10^6$  in helium are compared in figure 7 with air results obtained in a 14-inch Chance Vought hotshot tunnel and presented in reference 21.

The coefficients are referenced to the projected planform area of the basic ellipsoid. The pitching-moment coefficient is based on the body length with the moment reference center at 0.581. The angle of attack was measured relative to the model center line.

Although the Reynolds number for the helium results is an order of magnitude greater than the Reynolds number in air, a blunt body of this type has a relatively smaller contribution of skin-friction drag than the slender models discussed previously; as a result, there is better agreement between the air and helium axial-force coefficients. The normal-force and pitching-moment results are also in good agreement as seen in figure 7.

A comparison of the aerodynamic characteristics of the winged reentry capsule in a Mach number range of 15 to 20 and a Reynolds number range of  $0.1 \times 10^6$  to  $0.4 \times 10^6$  in air and at a Mach number of 24.1 and Reynolds number of  $1.74 \times 10^6$  in helium appears in figure 8.

The coefficients are based on the planform area of the model. In addition, the pitching-moment coefficient is based on the body length  $l$  with the moment reference center at 0.637 $l$ . The angle of attack was measured relative to the longitudinal axis. (See fig. 4(d).)

Within the scatter of the hotshot data there is good agreement between the  $C_N$  and  $C_m$  results obtained in air and helium. Again the agreement for  $C_A$  is better for this configuration than for the slender configurations.

Figure 9 presents the aerodynamic characteristics of the winged reentry glide vehicle. The air data were obtained in the 44-inch Boeing Airplane Company hotshot facility (designated BHS on figure) at Mach numbers of 22 and 16.4 and Reynolds number of  $0.0516 \times 10^6$  and  $0.142 \times 10^6$ , respectively. (See ref. 12.) The helium results were obtained at Mach numbers of 23.9 and 24.2 and at Reynolds numbers of  $2.138 \times 10^6$  and  $1.122 \times 10^6$ , respectively. Both sets of helium data were obtained under similar test conditions; the difference in the Reynolds number is due to the difference in the physical size of the two models tested.

The force and moment coefficients of the winged reentry glide vehicle are based on wing planform area and mean aerodynamic chord which are specified in figure 4(e) for both models. The angle of attack was measured relative to the longitudinal axis of the model.

With the exception of the  $M = 22$  data, the agreement between the air-helium results is good. Analysis of the data is complicated by the fact that all the models were tested in facilities with conical nozzles. Similar problems in data interpretation were encountered in investigations (refs. 22 to 24) employing conical nozzles.

#### Source Flow Effects

In addition to the results obtained in the  $5^\circ$  half-angle conical nozzle, data on the two hypersonic lifting configurations were obtained in the fully contoured nozzle in order to determine the extent of the effects of the source flow on the forces and moments.

A comparison of the aerodynamic characteristics of the winged reentry glider obtained in a conical nozzle at Mach numbers of 24.2 and 23.9 and Reynolds number of  $1.12 \times 10^6$  and  $2.138 \times 10^6$  and in a contoured nozzle at  $M = 20.5$  and a Reynolds number of  $1.46 \times 10^6$  is presented in figure 10. Both sets of data in the conical nozzle were obtained under similar test conditions. The difference in the Reynolds number was due to the difference in the physical size of the models.

The 0.016-scale model was aligned along the axis of the conical nozzle and rotated about a point at 67 percent of the body length measured from the nose. The 0.0305-scale model was aligned similarly but rotated about a point 65 percent of the body length measured from the nose.

The effects of using a conical nozzle to obtain force and moment data on the reentry glide vehicle can be seen in figure 10. The data obtained in the conical nozzle indicate a lower normal force and more positive pitching moment with increasing angle of attack compared with the data obtained in the contoured nozzle. Additional instability and less normal force at a given angle of attack resulted as the model length was increased.

A comparison of the aerodynamic characteristics of the reentry capsule presented in figure 11 indicates that conical flow effects are small for this particular test and model arrangement. For this test the model was mounted in the test section with the longitudinal axis of the model at zero angle of attack aligned along the axis of the nozzle, and it rotated about a point at 76 percent of the body length measured from the nose. As in references 23 and 24, the point about which a model pitches in source flow may determine the extent of the source flow effects. In view of this, the small differences between the conical data and contoured data may be attributed at least in part to the selection of the point of rotation.

#### CONCLUDING REMARKS

A comparison of the hypersonic longitudinal aerodynamic characteristics obtained in air and helium has been made for several lifting and nonlifting configurations. In addition, two lifting configurations were tested in both conical and contoured nozzles to determine the effects of source flow on aerodynamic forces and moments.

No appreciable effects of using helium as a test medium were noted in the normal-force coefficients, pitching-moment coefficients, or longitudinal stability characteristics in the angle-of-attack range of the tests. Essentially all the differences in axial-force coefficients and consequently in drag coefficients can be attributed to the difference in Reynolds numbers of the tests rather than to the effect of the differences in specific-heat ratios of the gases. Therefore, within the scope of this investigation, the use of helium as a test medium for aerodynamic investigations appears to be satisfactory at high Mach numbers for the ideal-gas case.

A comparison of force and moment data obtained in conical and contoured nozzles for one hypersonic lifting configuration indicated appreciable source flow effects which varied with model length. The data obtained on the second lifting configuration indicated small source flow effects which may be due at least in part to the position of the model in the flow field.

Langley Research Center,  
National Aeronautics and Space Administration,  
Langley Station, Hampton, Va., December 16, 1963.

## REFERENCES

1. Henderson, Arthur, Jr., and Johnston, Patrick J.: Fluid-Dynamic Properties of Some Simple Sharp- and Blunt-Nosed Shapes at Mach Numbers From 16 to 24 in Helium Flow. NASA MEMO 5-8-59L, 1959.
2. Mueller, James N., Close, William H., and Henderson, Arthur, Jr.: An Investigation of Induced-Pressure Phenomena on Axially Symmetric, Flow-Alined, Cylindrical Models Equipped With Different Nose Shapes at Free-Stream Mach Numbers From 15.6 to 21 in Helium. NASA TN D-373, 1960.
3. Henderson, Arthur, Jr.: Investigation of the Flow Over Simple Bodies at Mach Numbers of the Order of 20. NASA TN D-449, 1960.
4. Bertram, Mitchel H., and Blackstock, Thomas A.: Some Simple Solutions to the Problem of Predicting Boundary-Layer Self-Induced Pressures. NASA TN D-798, 1961.
5. Vas, I. E., and Bogdonoff, S. M.: Hypersonic Studies of Blunt Unswept Wings. Rep. No. 450 (WADC TN 59-127, AD 214 623), Dept. Aero. Eng., Princeton Univ., Apr. 1959.
6. Vas, I. E., and Bogdonoff, S. M.: Mach and Reynolds Number Effects on the Flows Over Blunt Flat Plates at Hypersonic Speeds. Rep. No. 529 (ARL Tech Note 60-164), Dept. Aero. Eng., Princeton Univ., Nov. 1960.
7. Vas, I. E., Bogdonoff, S. M., and Hammitt, A. G.: An Experimental Investigation of the Flow Over Simple Two-Dimensional and Axial Symmetric Bodies at Hypersonic Speeds. Rep. No. 382 (WADC TN 57-246), Dept. Aero. Eng., Princeton Univ., June 1957.
8. Witcofski, Robert D., and Henderson, Arthur, Jr.: Induced Pressures on Cylindrical Rods With Various Nose Drags and Nose Shapes at Mach Numbers of 17 and 21. NASA TN D-1266, 1962.
9. Wagner, Richard D., Jr., Pine, W. Clint, and Henderson, Arthur, Jr.: Laminar Heat-Transfer and Pressure-Distribution Studies on a Series of Reentry Nose Shapes at a Mach Number of 19.4 in Helium. NASA TN D-891, 1961.
10. Johnson, Robert H.: Helium Tunnel. Doc. No. 62SD592 (Contract AF 04(647)-617), Missile and Space Vehicle Dept., Gen. Elec. Co., May 29, 1962.
11. Johnston, Patrick J., and Snyder, Curtis D.: Static Longitudinal Stability and Performance of Several Ballistic Spacecraft Configurations in Helium at a Mach Number of 24.5. NASA TN D-1379, 1962.

12. Henderson, Arthur, Jr.: Recent Investigations of the Aerodynamic Characteristics of General and Specific Lifting and Nonlifting Configurations at Mach 24 in Helium, Including Air-Helium Simulation Studies. Presented at the Specialists' Meeting on the High Temperature Aspects of Hypersonic Flow (Rhode-Saint-Genese, Belgium), AGARD, Apr. 1962.
13. Love, Eugene S., Henderson, Arthur, Jr., and Bertram, Mitchel H.: Some Aspects of Air-Helium Simulation and Hypersonic Approximations. NASA TN D-49, 1959.
14. Ladson, Charles L.: Effects of Several Nose and Vertical-Fin Modifications on the Low-Angle-of-Attack Static Stability of a Winged Reentry Vehicle at Mach Numbers of 9.6 in Air and 17.8 in Helium. NASA TN X-608, 1961.
15. Mueller, James N.: Conversion of Inviscid Normal-Force Coefficients in Helium to Equivalent Coefficients in Air for Simple Shapes at Hypersonic Speeds. NACA TN 3807, 1956.
16. Erickson, Wayne D.: Real-Gas Correction Factors for Hypersonic Flow Parameters in Helium. NASA TN D-462, 1960.
17. Swalley, Frank E.: Measurement of Flow Angularity at Supersonic and Hypersonic Speeds With the Use of a Conical Probe. NASA TN D-959, 1961.
18. Monaghan, R. J.: An Approximate Solution of the Compressible Laminar Boundary Layer on a Flat Plate. R. & M. No. 2760, British A.R.C., 1956.
19. Cheng, Hsien K.: Hypersonic Shock-Layer Theory of a Yawed Cone and Other Three-Dimensional Pointed Bodies. WADC TN 59-335, U.S. Air Force, Oct. 1959. Errata, June 1960.
20. Ladson, Charles L., and Blackstock, Thomas A.: Air-Helium Simulation of the Aerodynamic Force Coefficients of Cones at Hypersonic Speeds. NASA TN D-1473, 1962.
21. Russell, C. P., Jr.: Comparison of Test Results With Calculated Aerodynamic Coefficients for Four Entry Vehicles. AST/EIR-13292, Vought Astronautics, Jan. 1961.
22. Baradell, Donald L., and Bertram, Mitchel H.: The Blunt Plate in Hypersonic Flow. NASA TN D-408, 1960.
23. Whitfield, Jack D., and Norfleet, Glenn D.: Source Flow Effects in Conical Hypervelocity Nozzles. AEDC TDR-62-116 (Contract No. AF 40(600)-800 S/A 24(61-73)), Arnold Eng. Dev. Center, June 1962.
24. Burke, A. F., and Bird, K. D.: The Use of Conical and Contoured Expansion Nozzles in Hypervelocity Facilities. Rep. No. CAL-112, Cornell Aero. Lab., Inc., Mar. 1962. (Rev. July 1962.)

CONFIDENTIAL

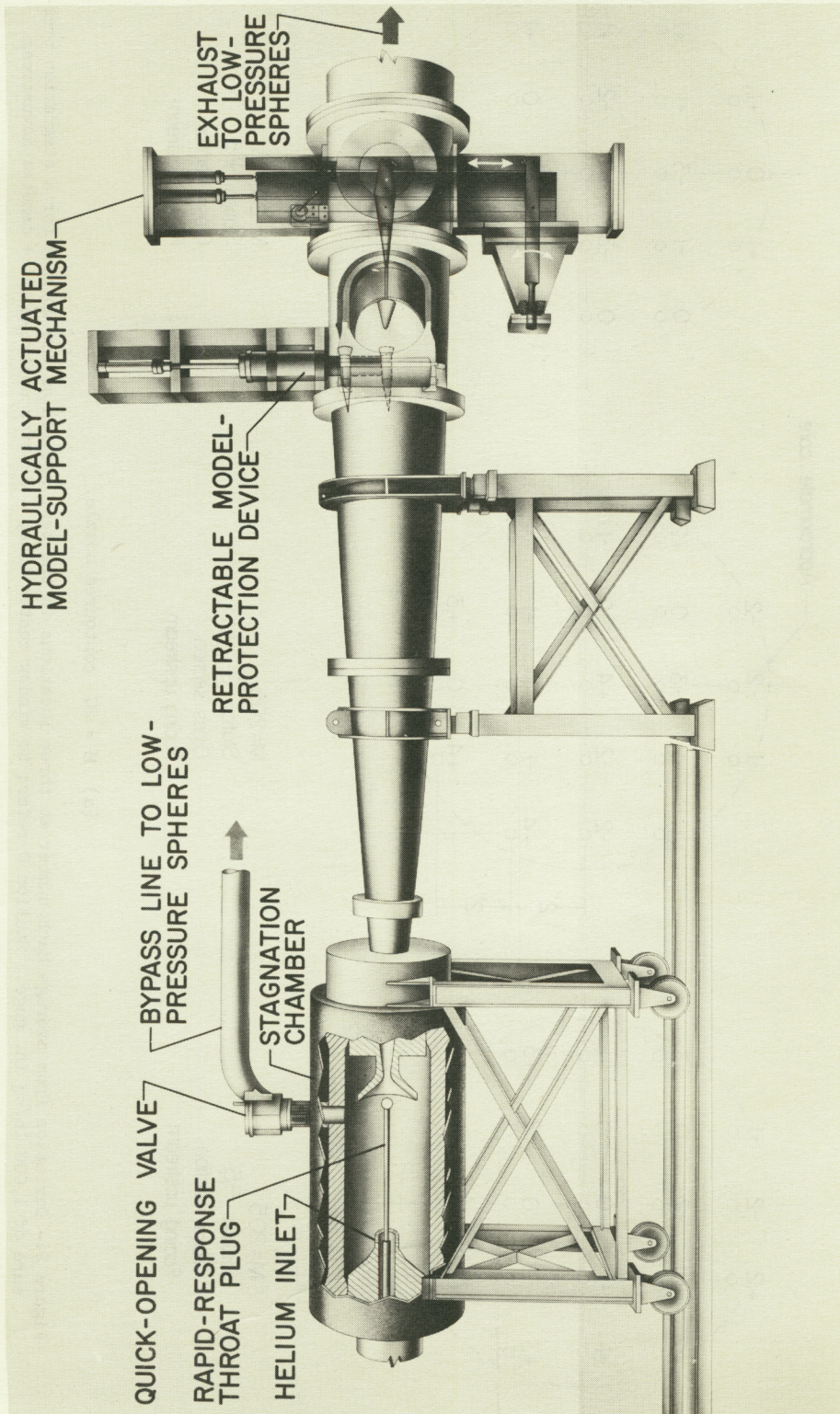
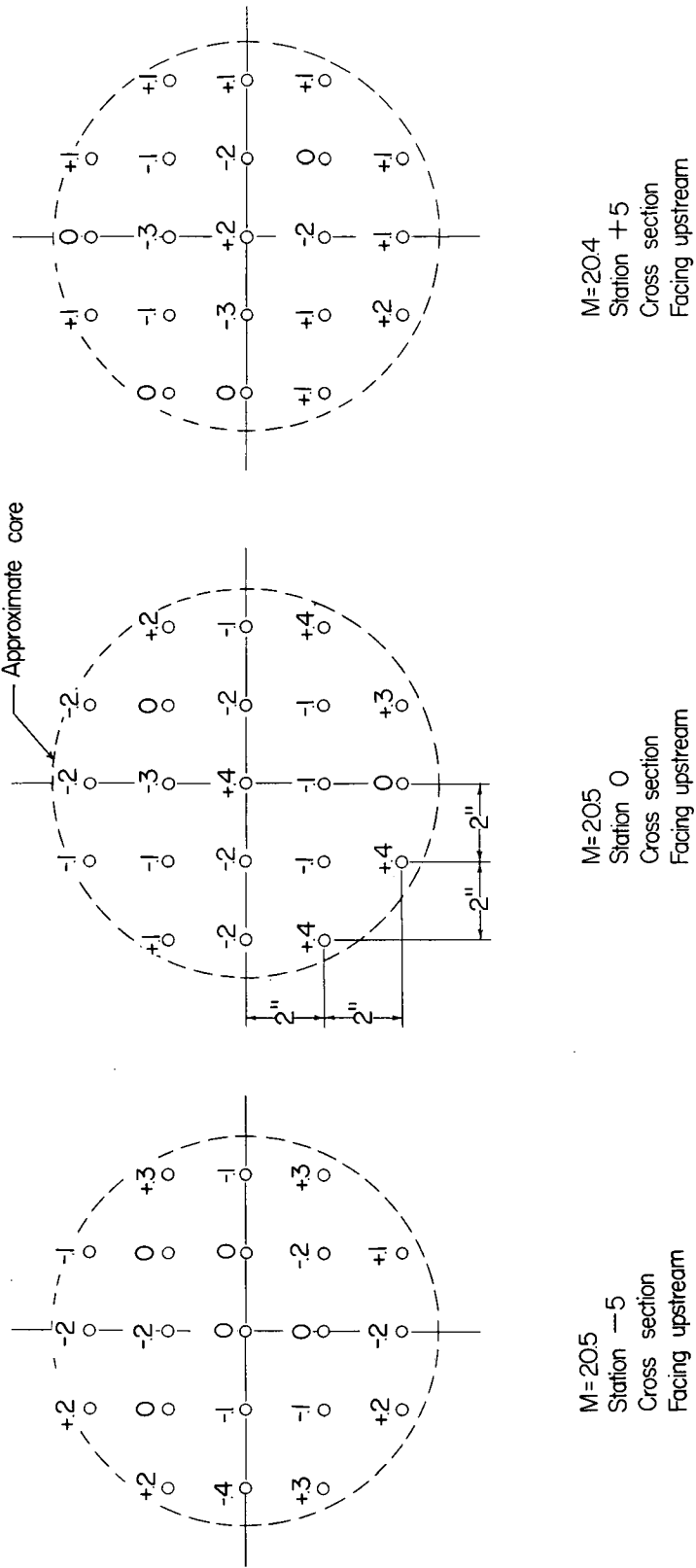


Figure 1.- Langley 22-inch helium tunnel with  $M = 20$  contoured nozzle.

L-1718

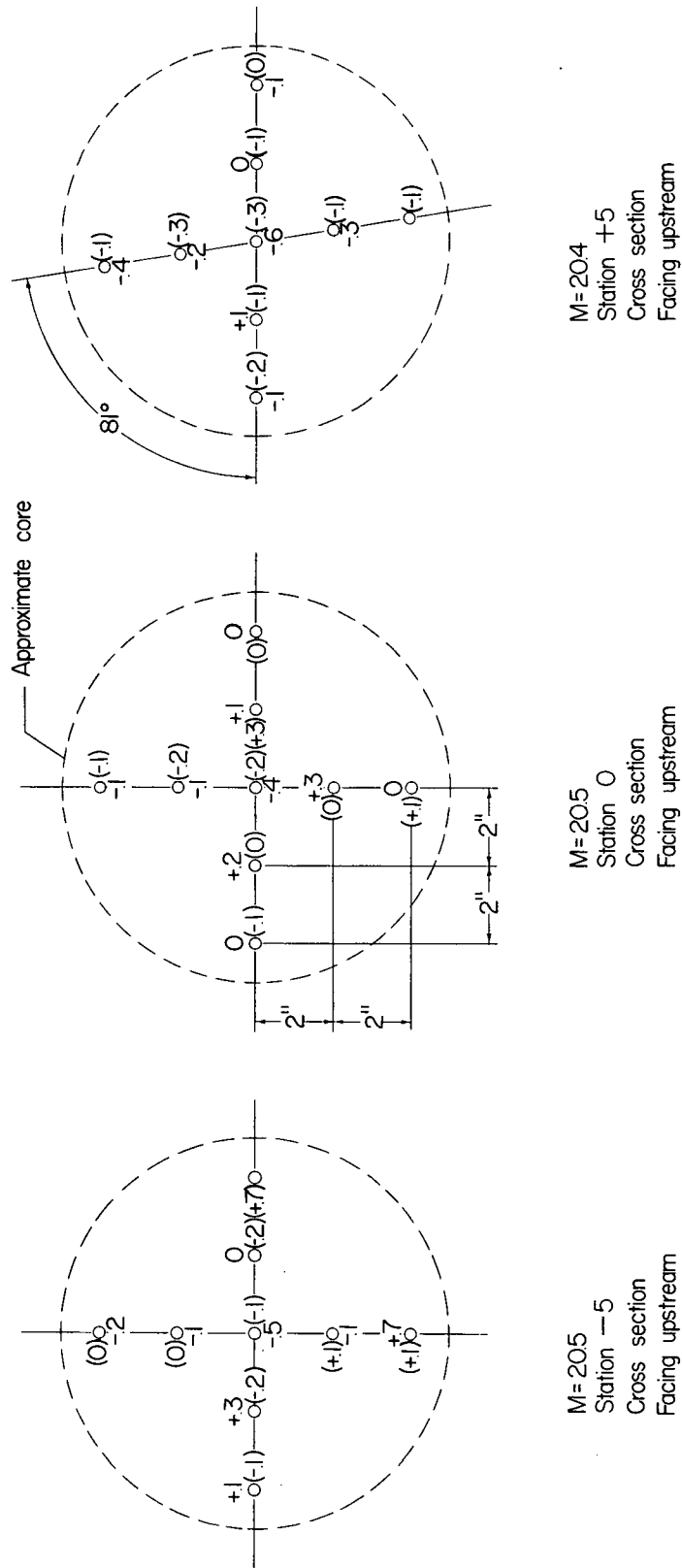
CONFIDENTIAL



(a) M = 20 contoured nozzle.

Figure 2.- Deviation from average Mach number at three locations in the test section of the nozzles for a stagnation pressure of 1,000 lb/sq in. gage. Station 0 refers to window center line; - denotes upstream and + denotes downstream.

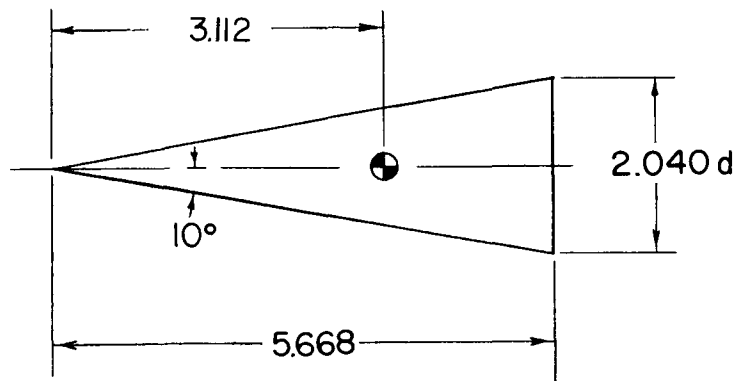




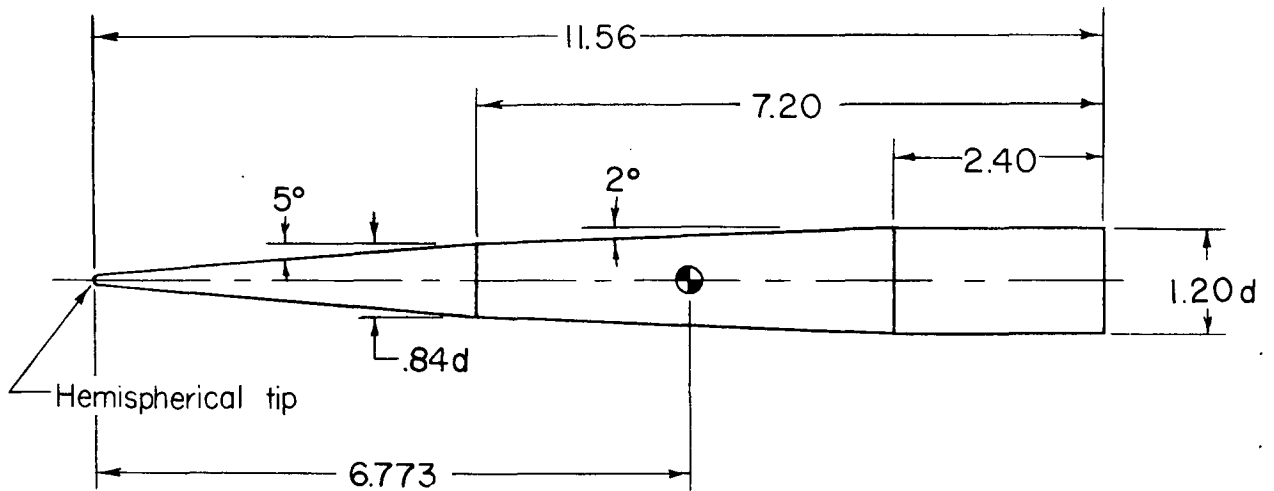
(a)  $M = 20$  contoured nozzle for a stagnation pressure of 1,000 lb/sq in. gage.

Figure 3.- Flow angularity in test section. Station 0 refers to the center of the window; - denotes upstream and + denotes downstream.  $\sigma$  is 0.0 angle of sidewash and  $\epsilon$  is 0.0 angle of downwash.



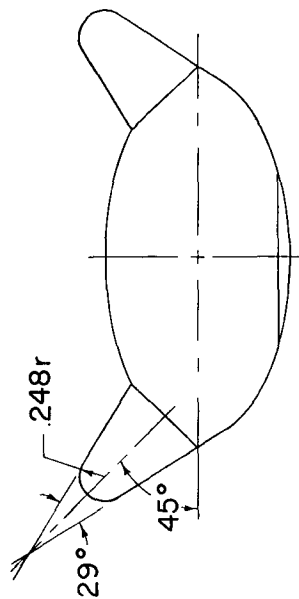
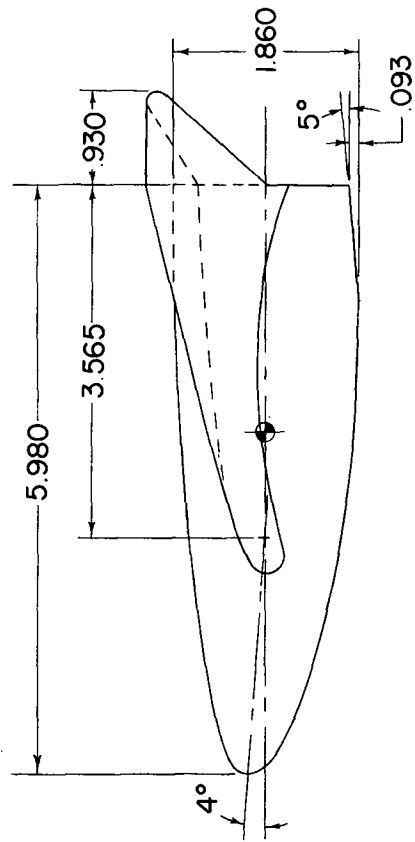
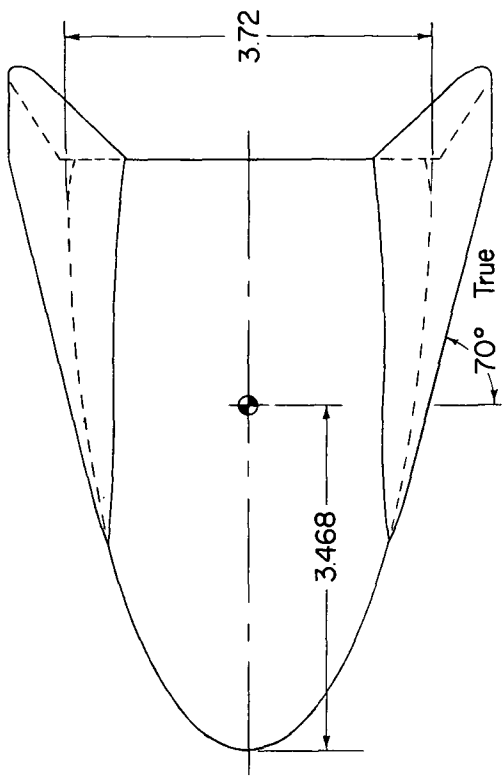


(a)  $10^\circ$  cone.  $S = 3.27$ ;  $l = 2.04$ .



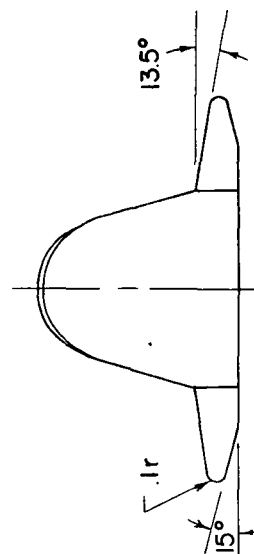
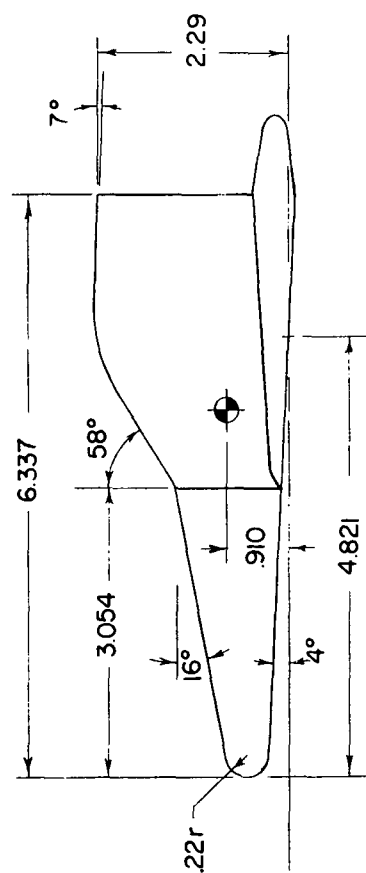
(b) Slender conical configuration.  $S = 1.13$ ;  $l = 1.20$ .

Figure 4.- Model drawings. All linear dimensions are in inches.



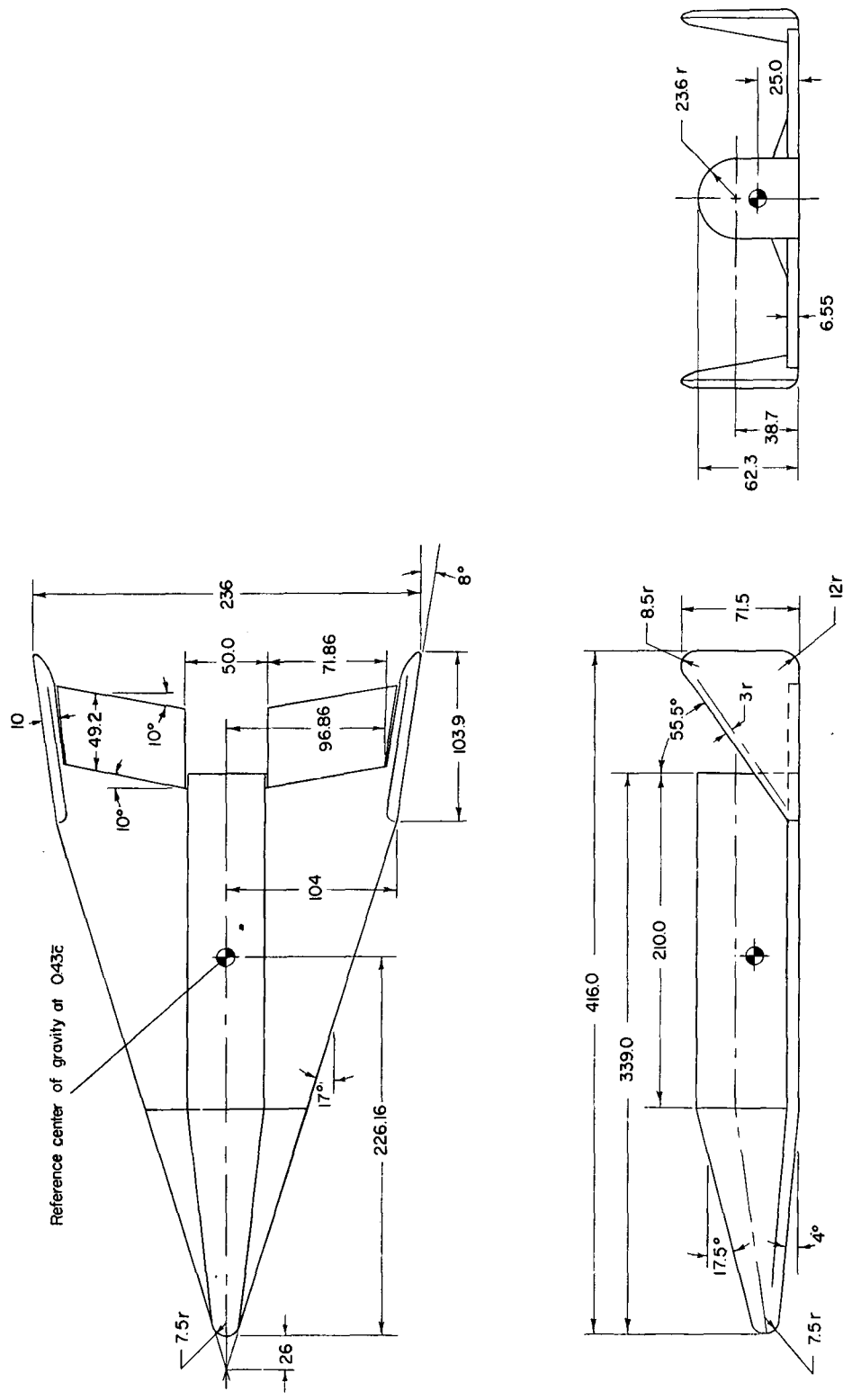
(c) 0.062-scale winged ellipsoid.  $S = 17.416$ ;  $l = 5.98$ ;  $b = 3.72$ .

Figure 4.- Continued.



(d) 0.035-scale winged reentry capsule.  $S = 14.9$ ;  $l = 6.337$ ;  $b = 4.80$ .

Figure 4.- Continued.



(e) Winged reentry glider vehicle. 0.016-scale model:  $S = 12.49$  and  $\bar{c} = 4.06$ . 0.0305-scale model:  $S = 45.38$  and  $\bar{c} = 7.03$ .

Figure 4.- Concluded.

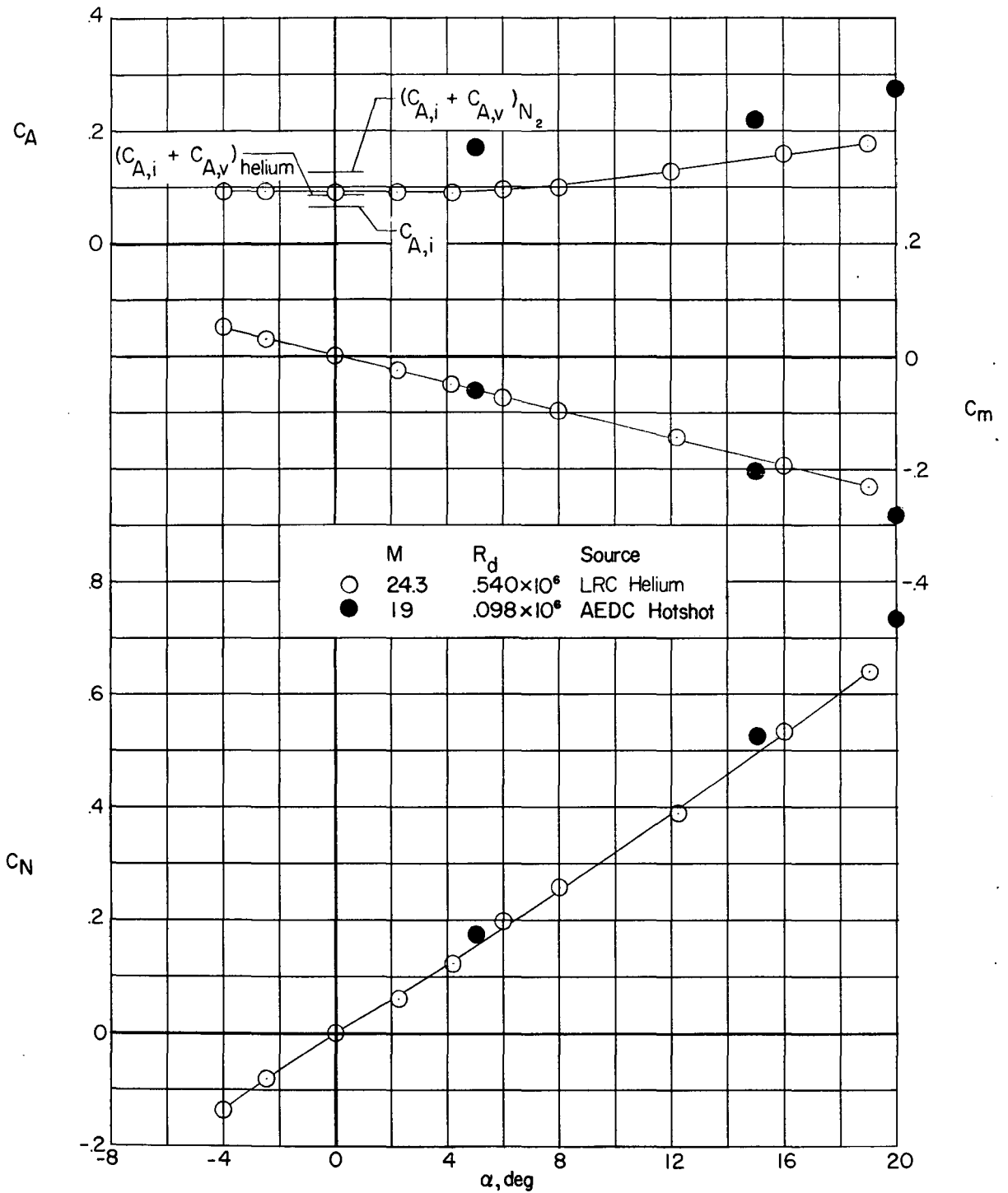


Figure 5.- Aerodynamic characteristics of  $10^\circ$  cone in conical nozzle. Data obtained in Langley 22-inch helium tunnel (designated LRC) and in the Von Karman facility of Arnold Engineering Development Center.

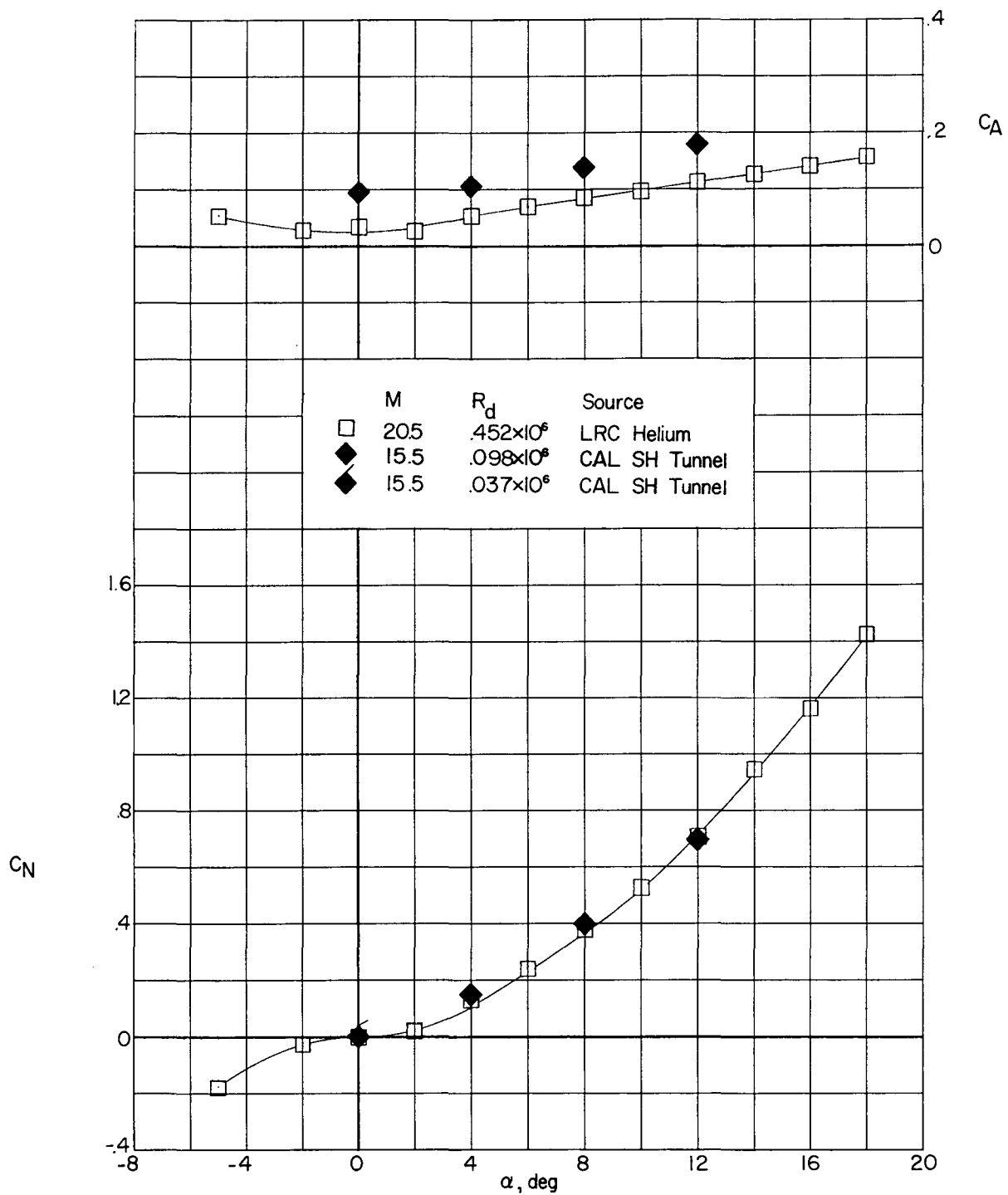


Figure 6.- Aerodynamic characteristics of slender conical configuration in contoured nozzle. Data obtained in the Langley 22-inch helium tunnel and in the Cornell Aeronautical Laboratory 48-inch shock tunnel.

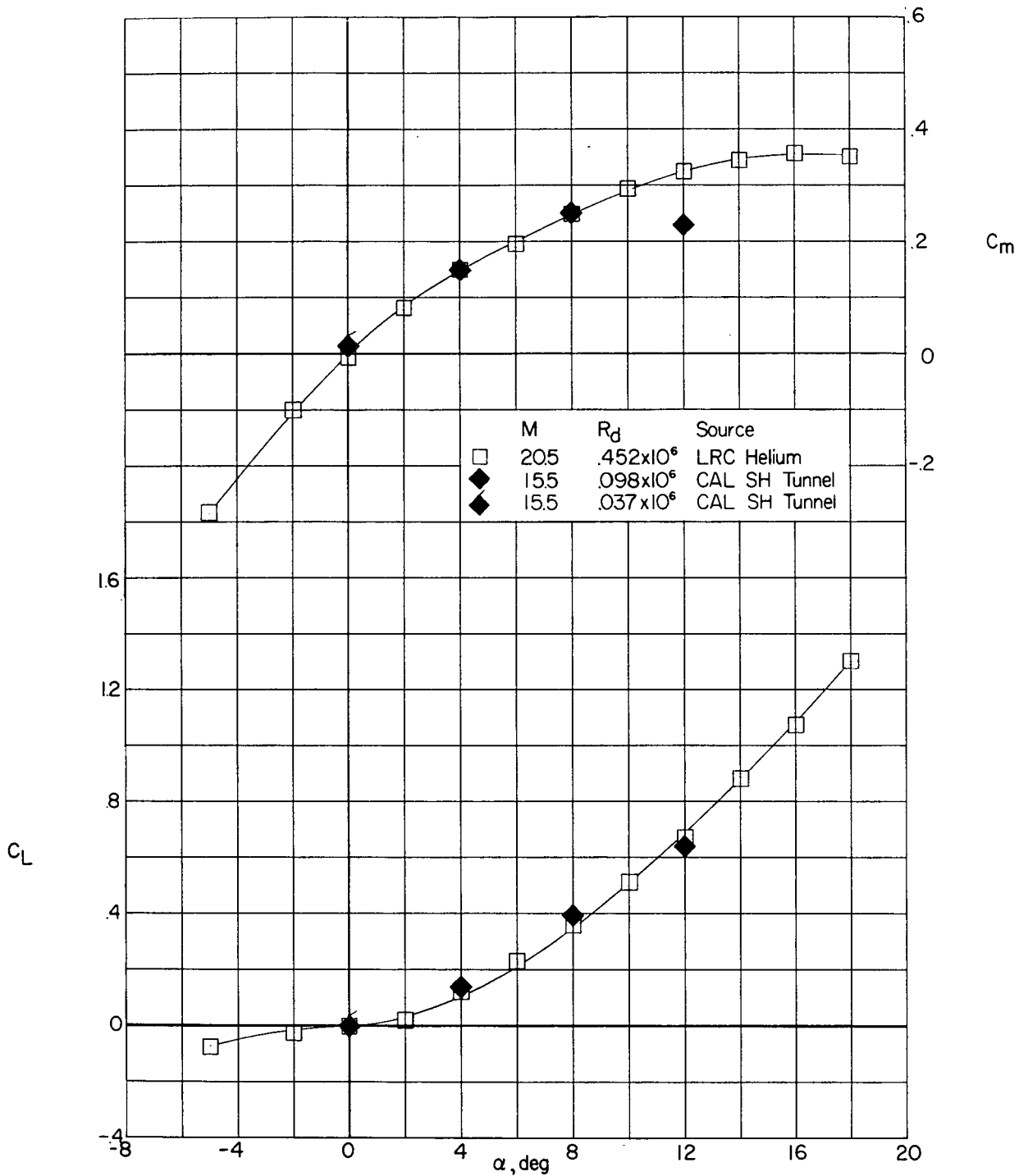


Figure 6.- Continued.

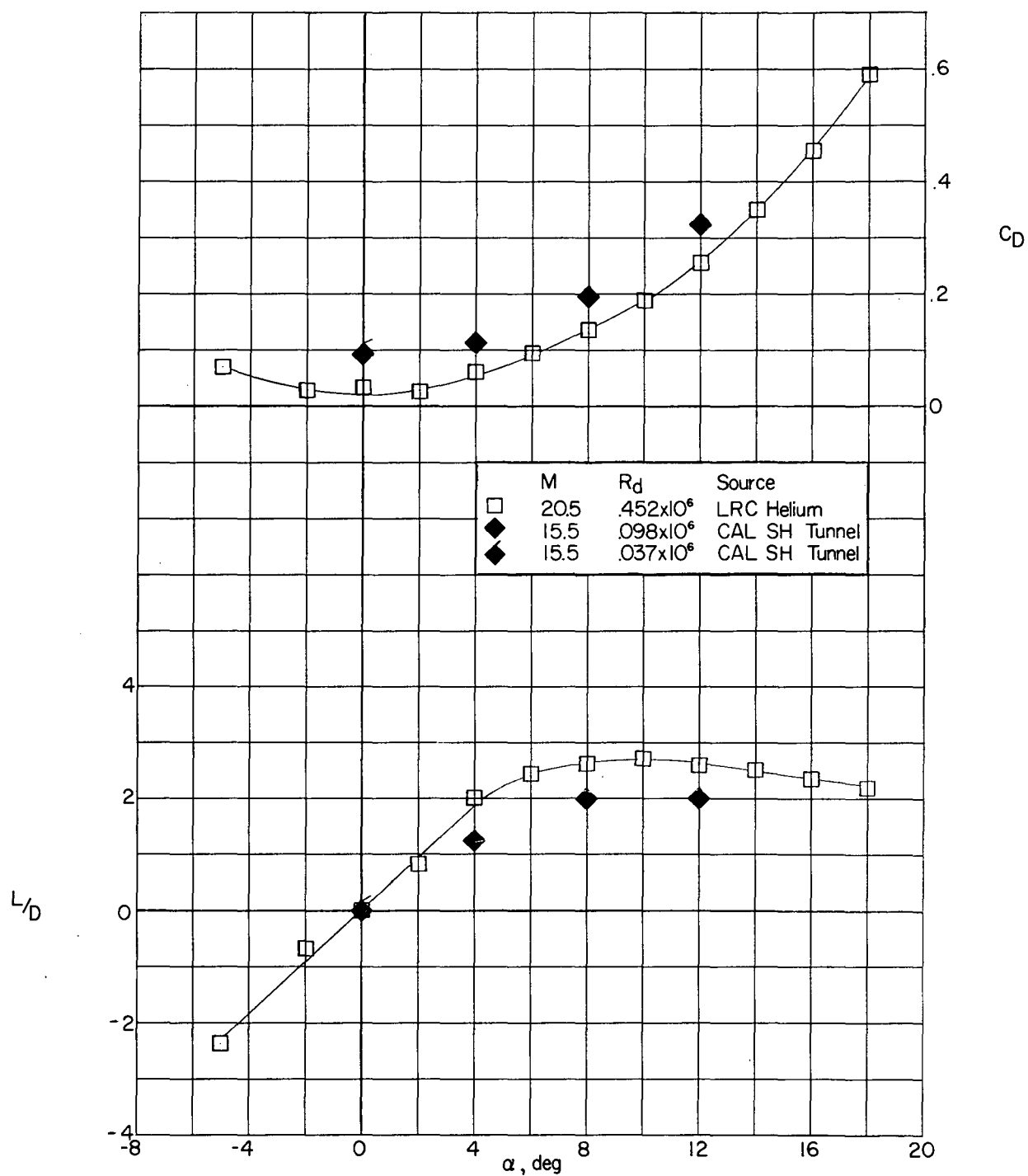


Figure 6.- Concluded.

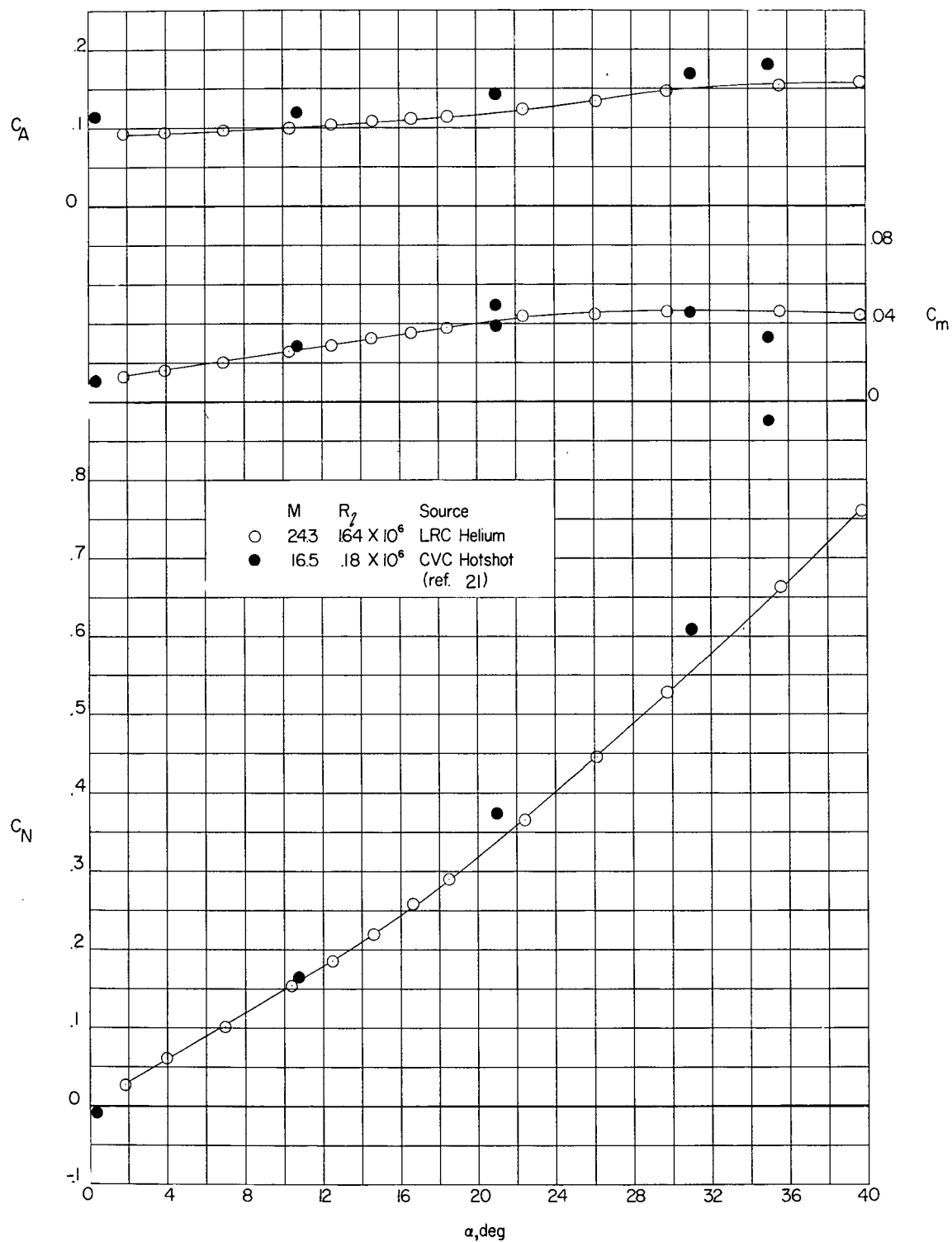


Figure 7.- Aerodynamic characteristics of winged ellipsoid in conical nozzle.

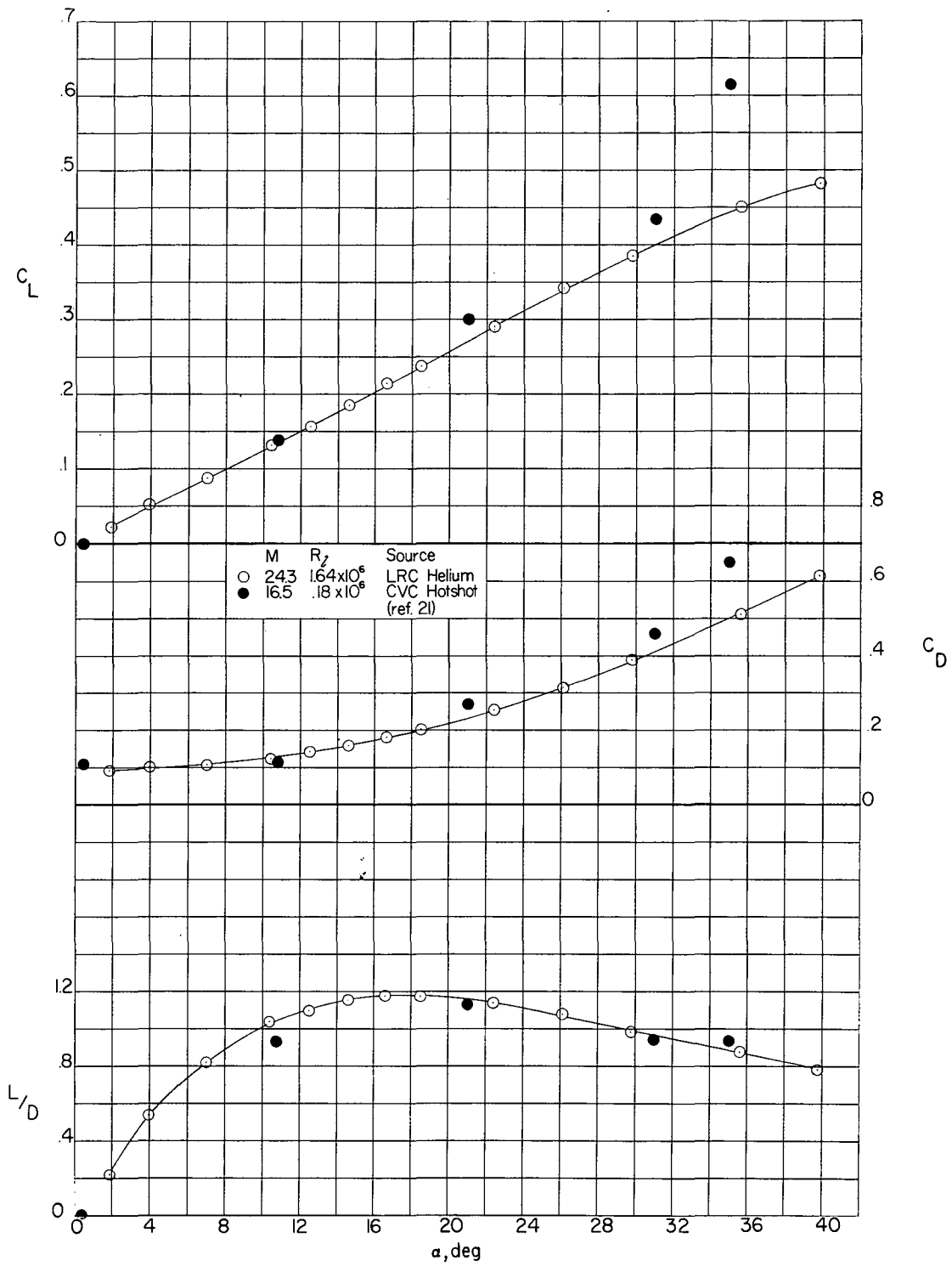


Figure 7.- Continued.

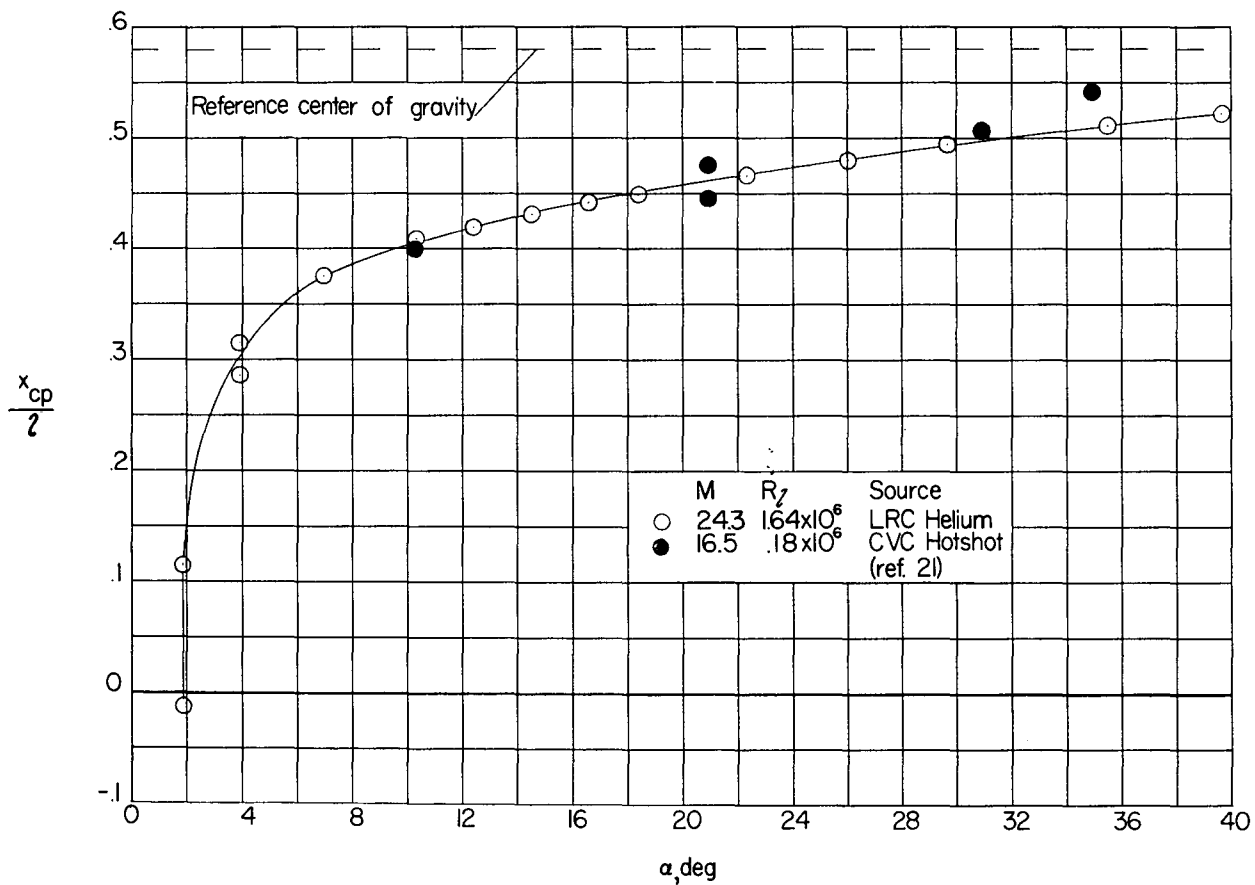
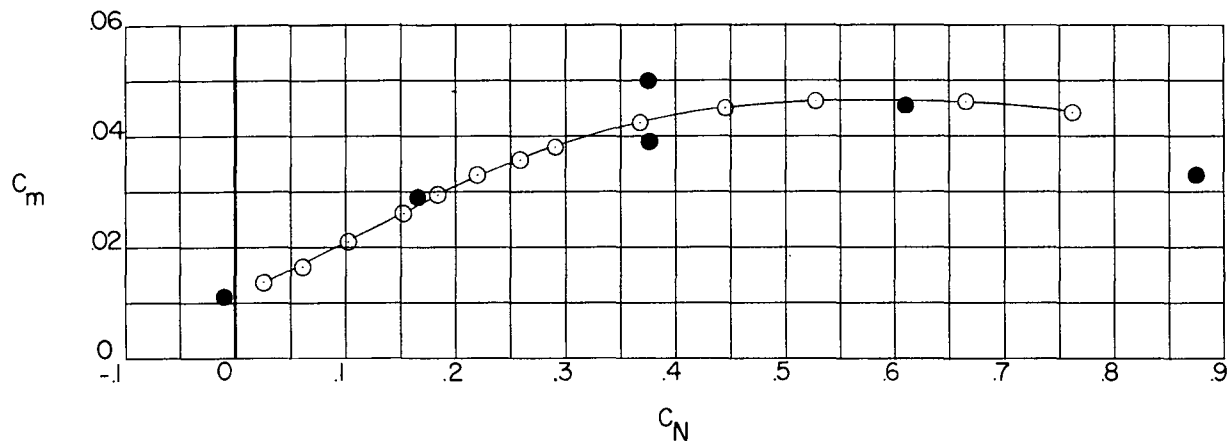


Figure 7.- Concluded.

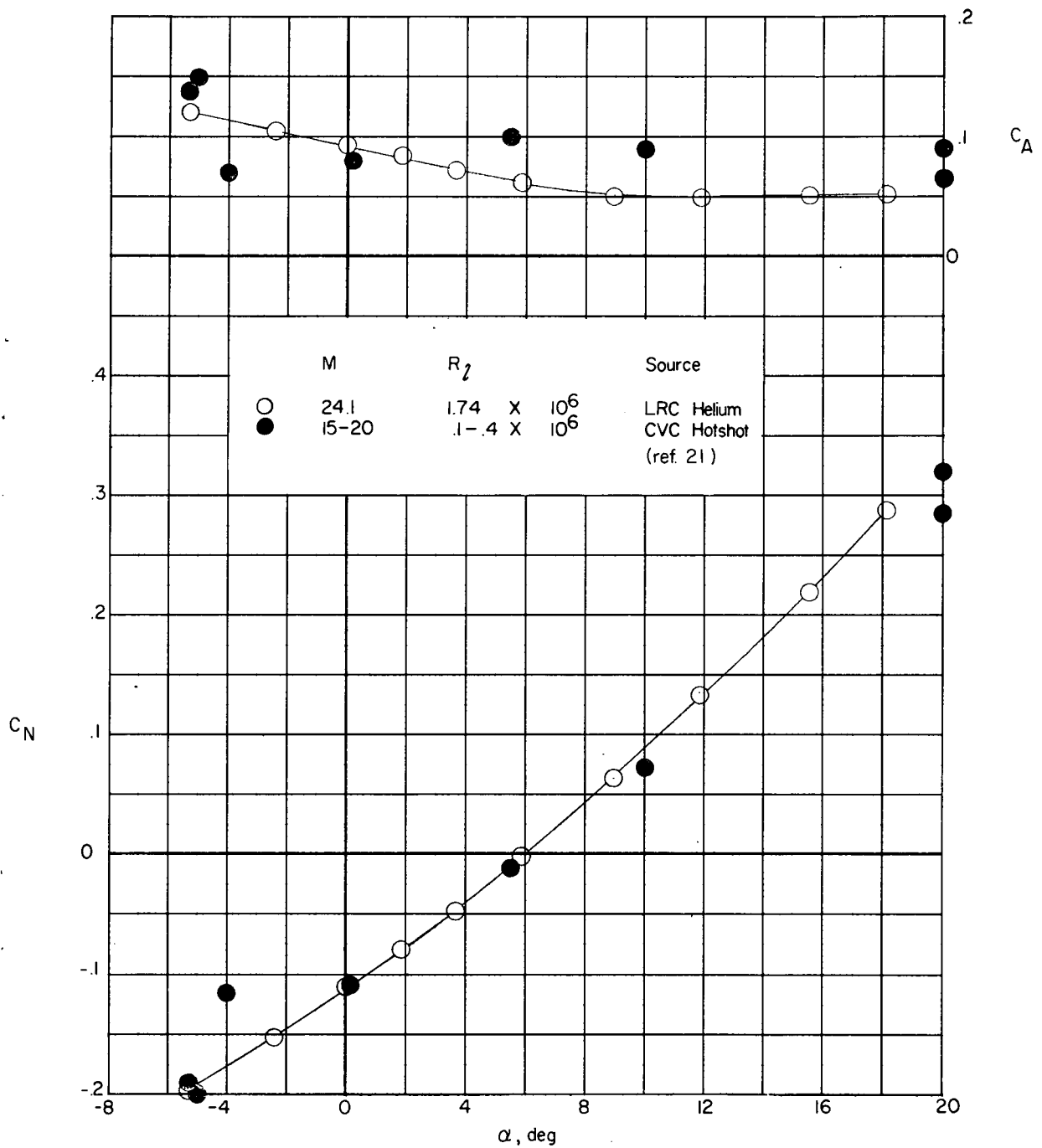


Figure 8.- Aerodynamic characteristics of winged reentry vehicle in conical nozzle.

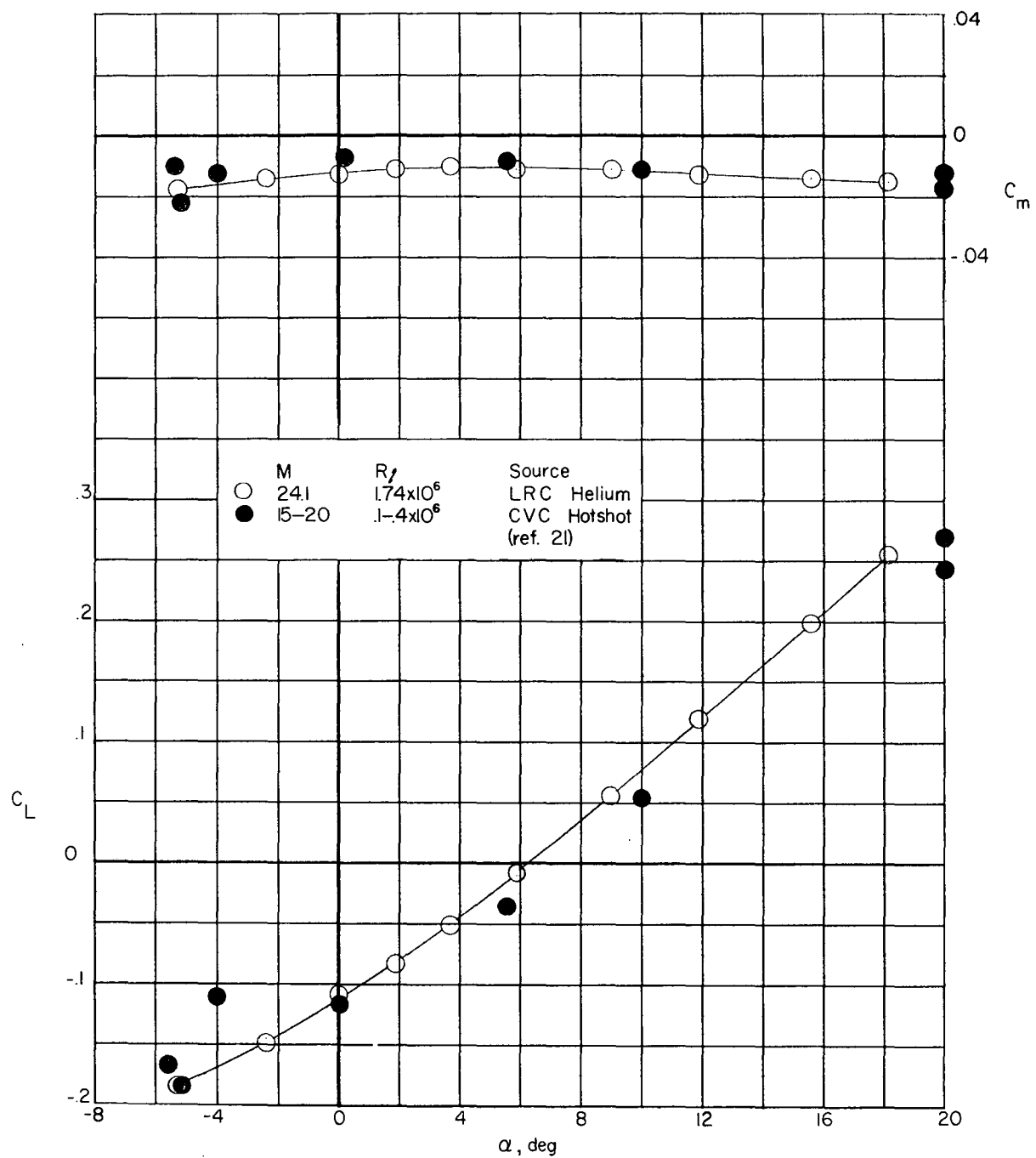


Figure 8.- Continued.

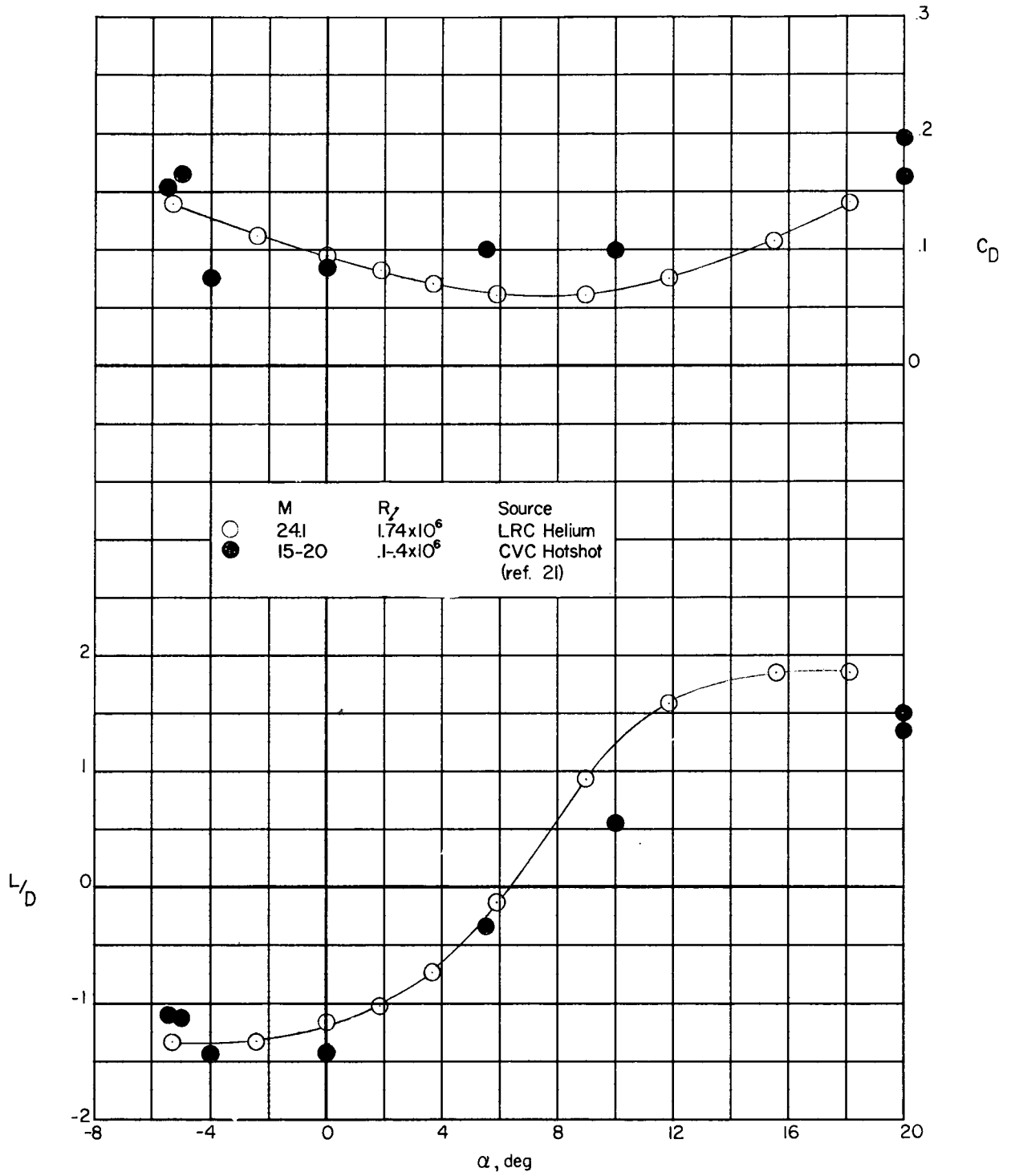


Figure 8.- Continued.

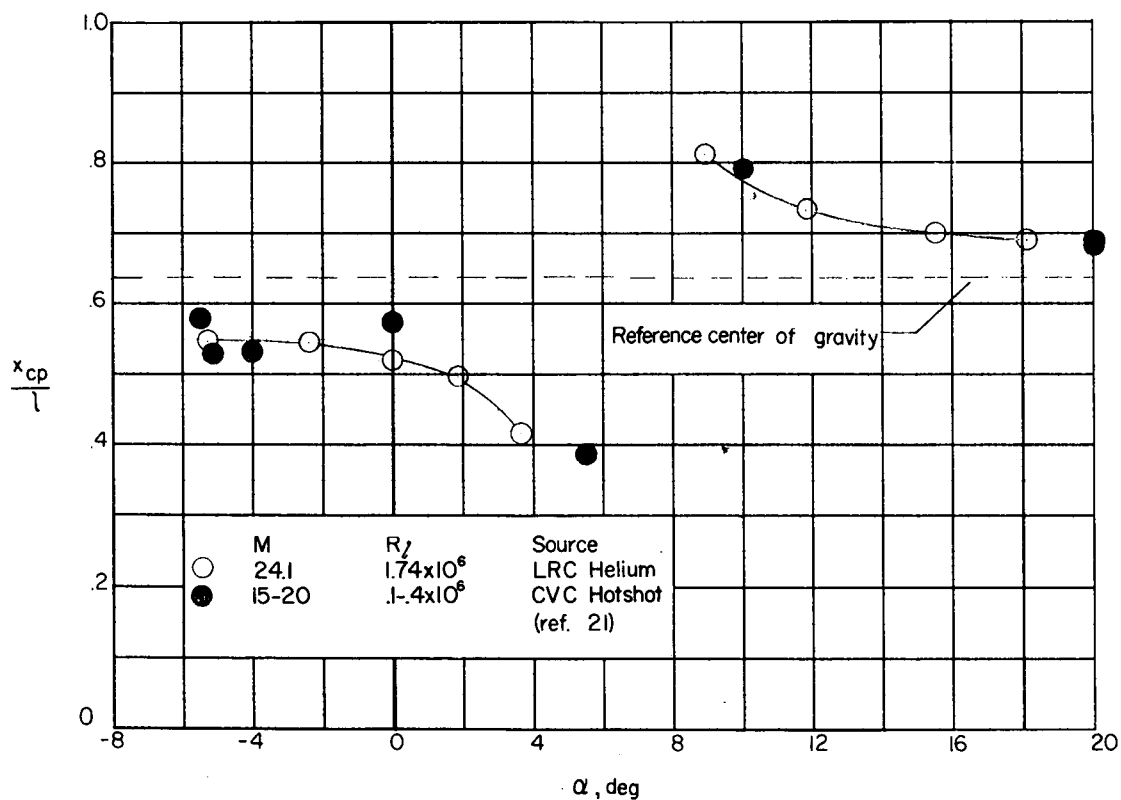
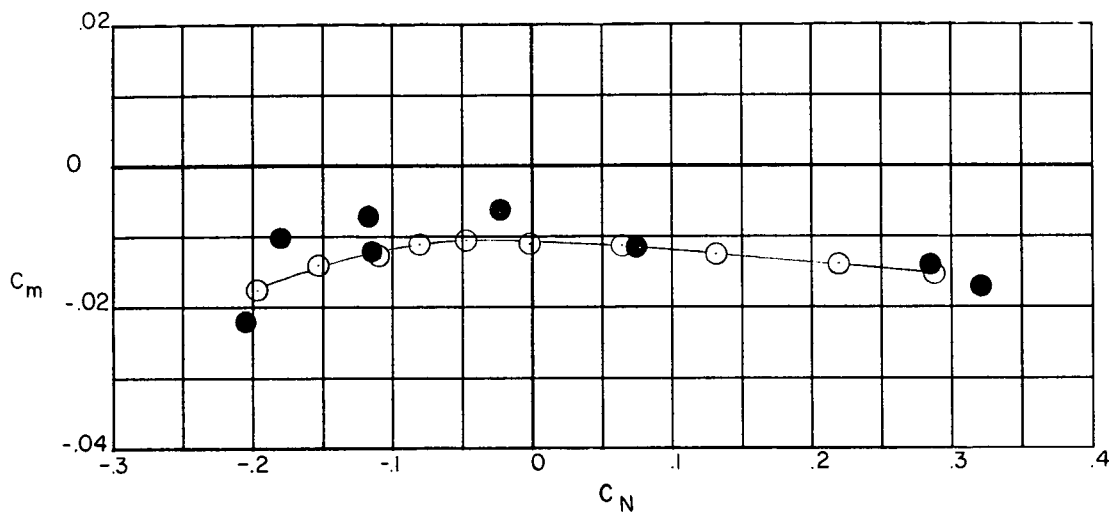


Figure 8.- Concluded.

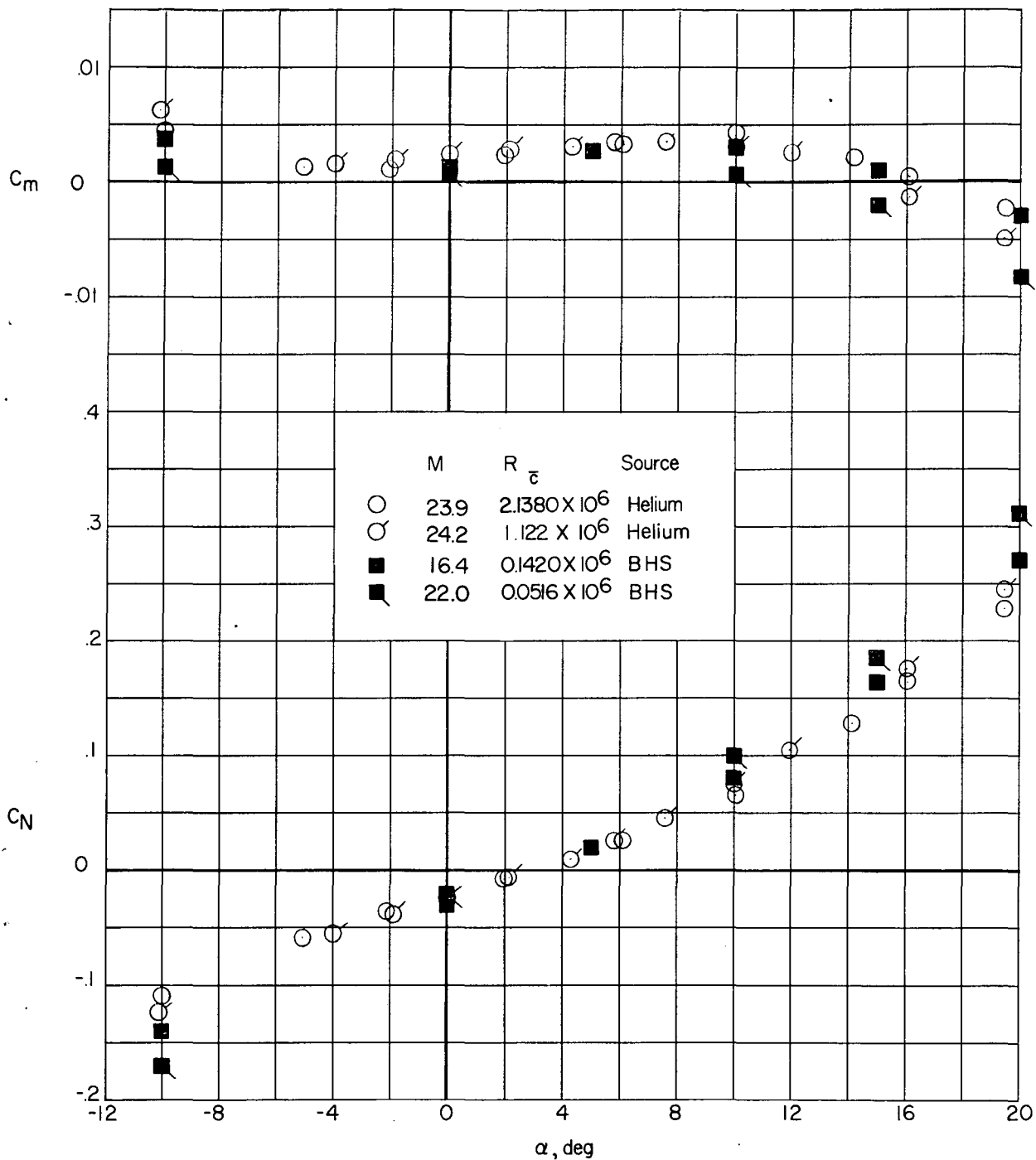


Figure 9.- Aerodynamic characteristics of winged reentry glider configuration in conical nozzle. Data obtained in the Langley 22-inch helium tunnel and in the 44-inch Boeing Airplane Company hotshot facility.

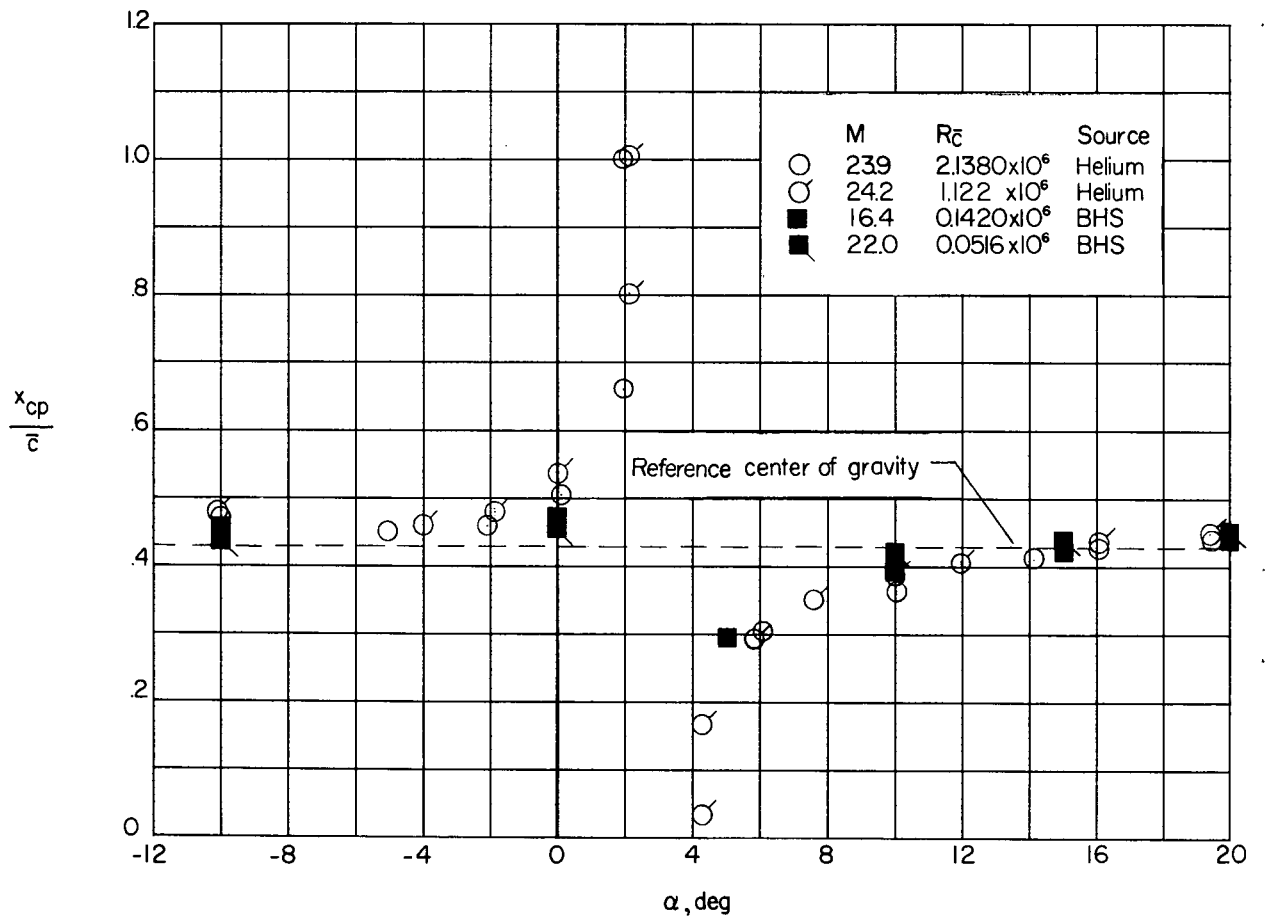
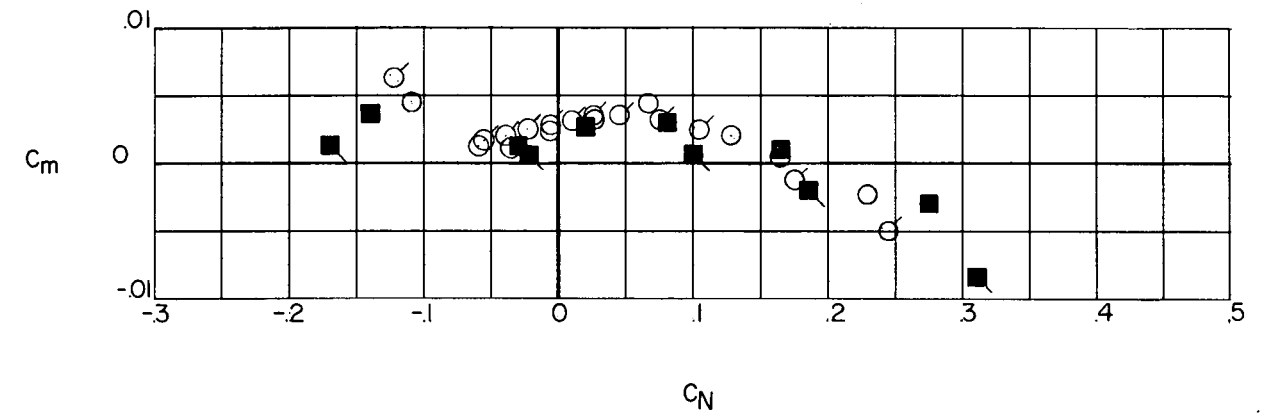


Figure 9.- Concluded.

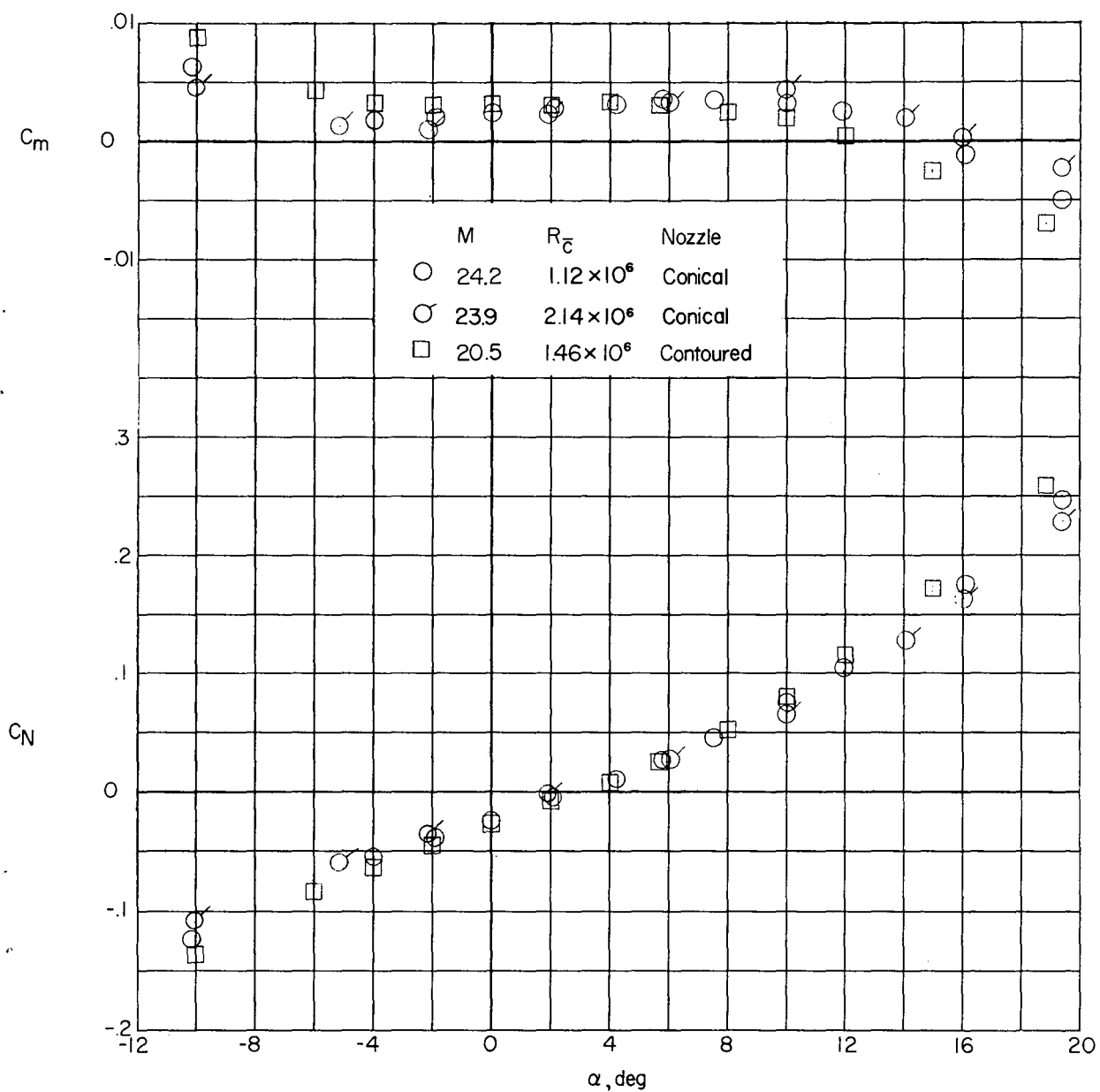


Figure 10.- Aerodynamic characteristics of winged reentry glider configuration in contoured and conical nozzles.

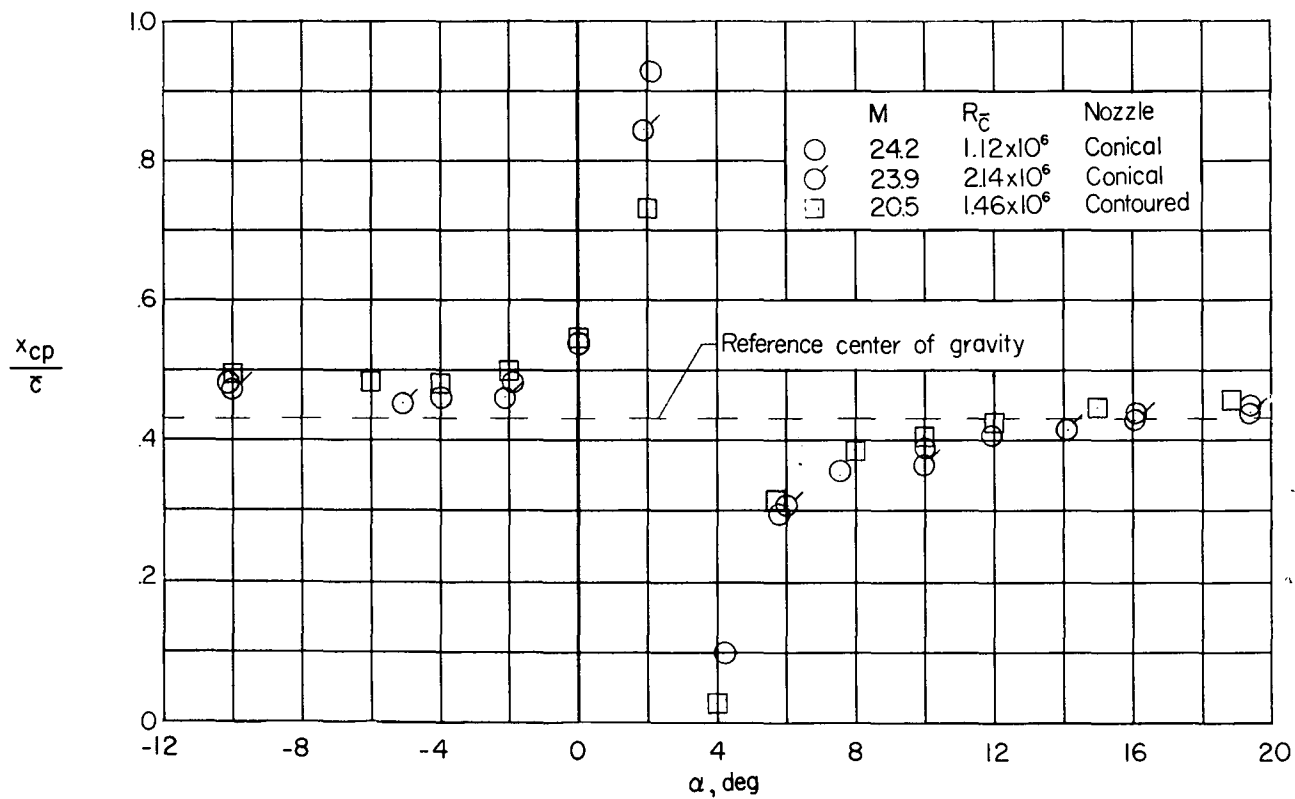
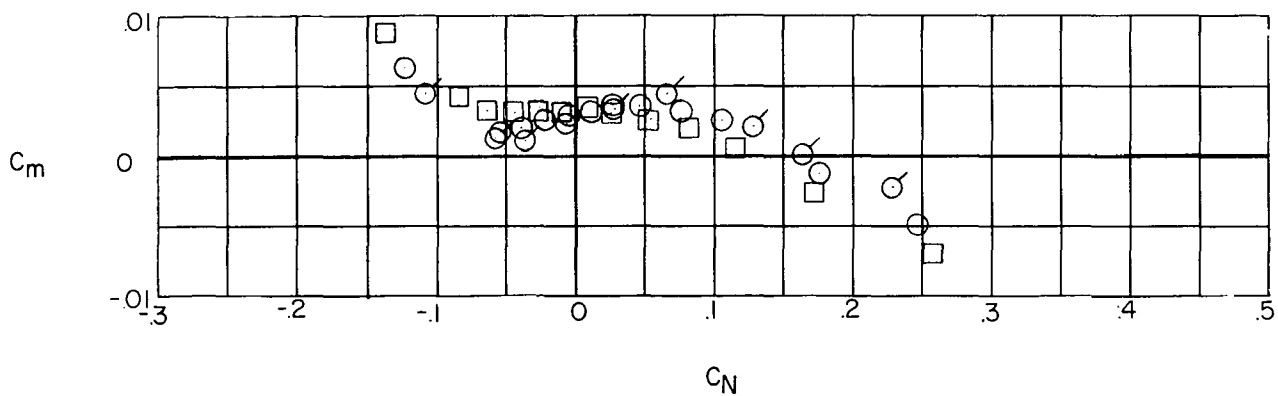


Figure 10.- Concluded.

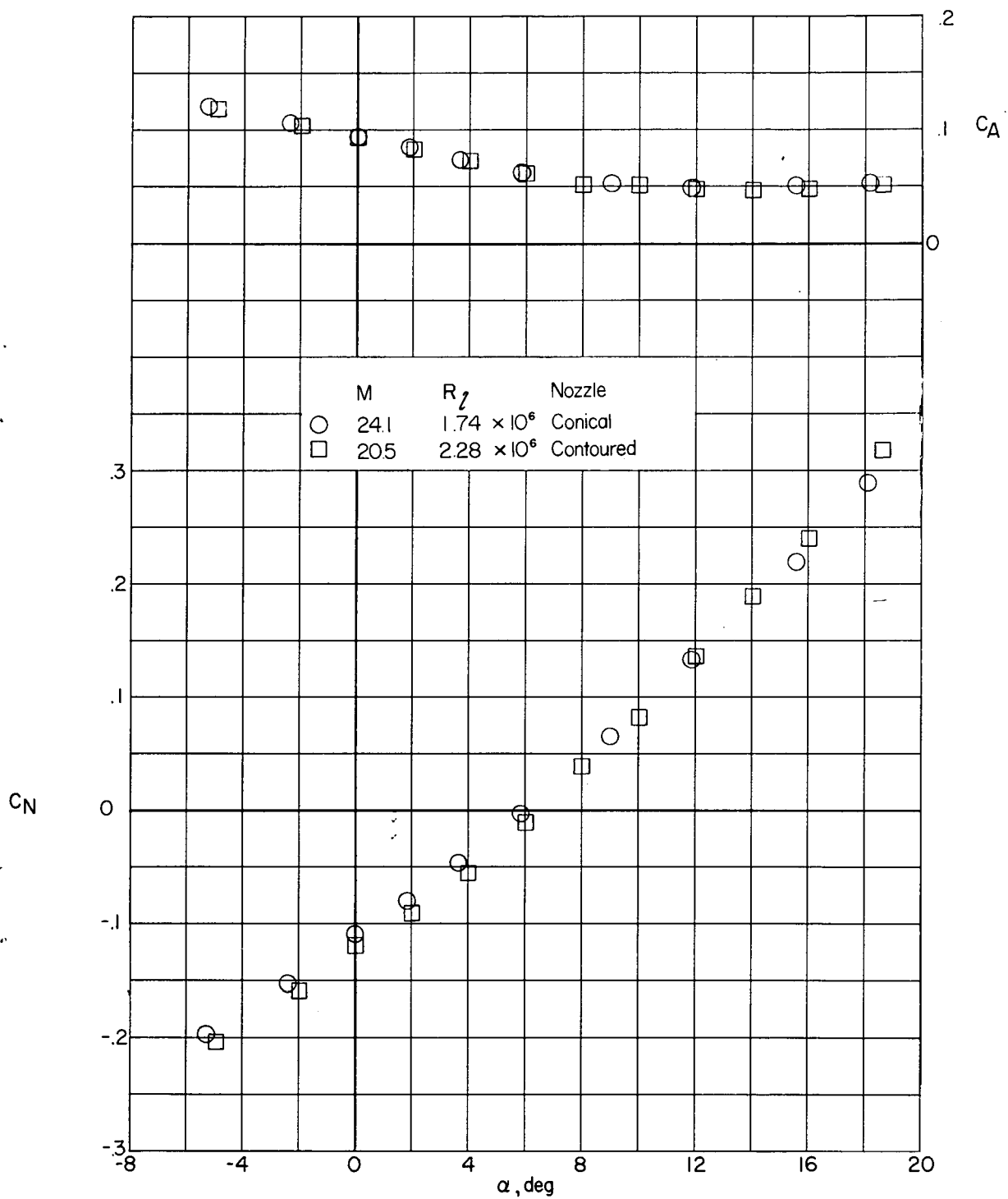


Figure 11.- Aerodynamic characteristics of winged reentry vehicle obtained in contoured and conical nozzles.

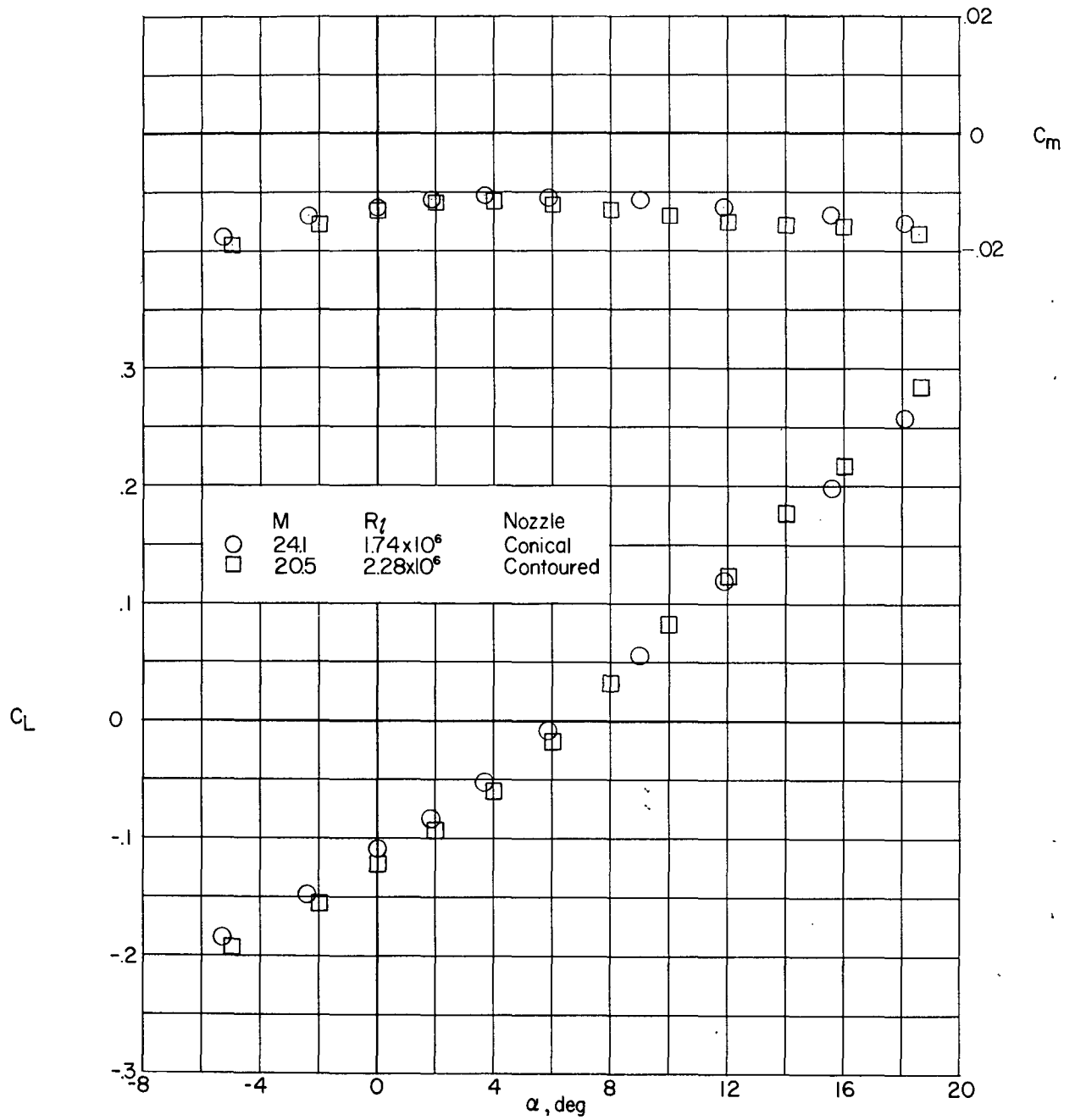


Figure 11.- Continued.

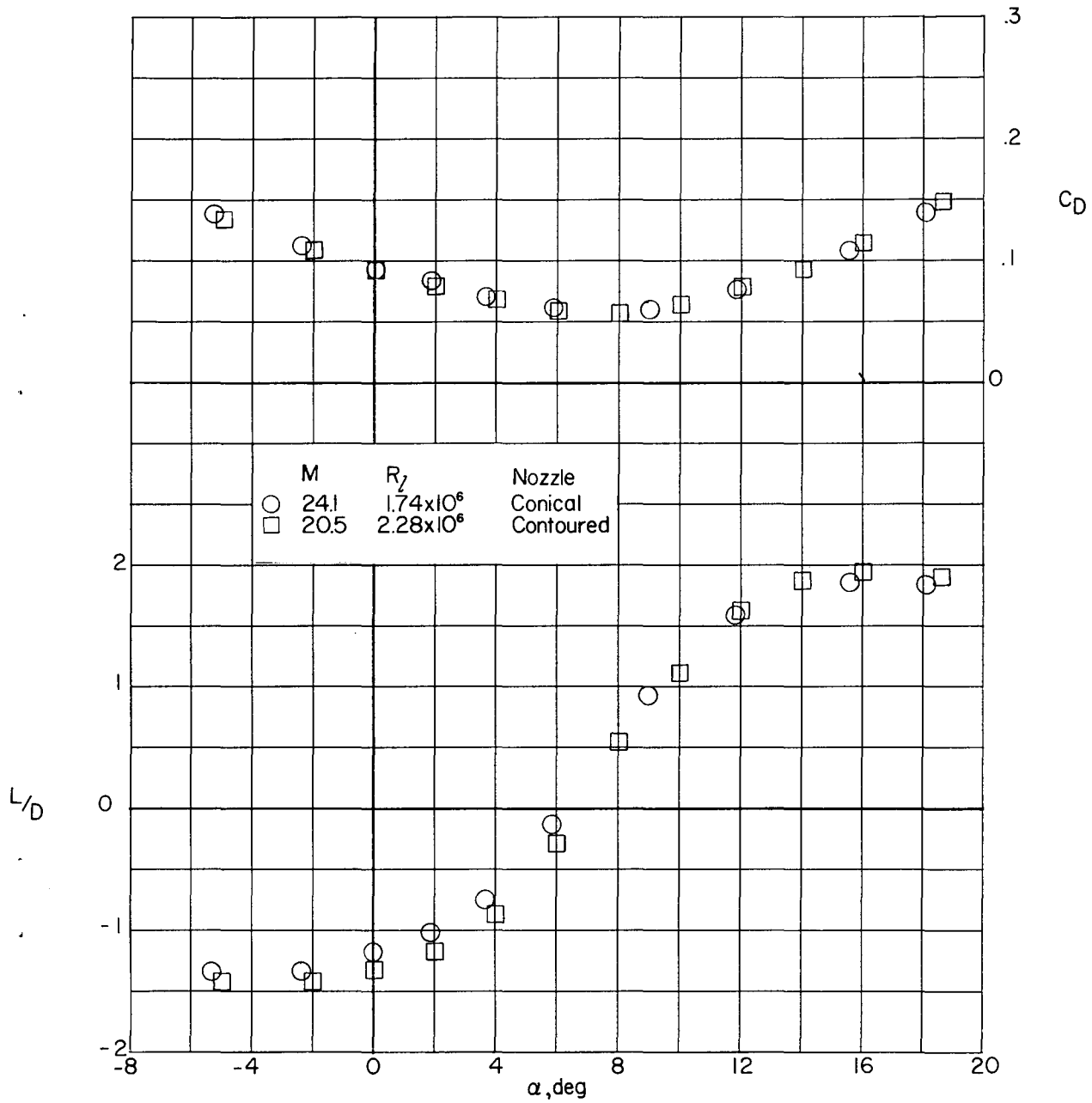


Figure 11.- Continued.

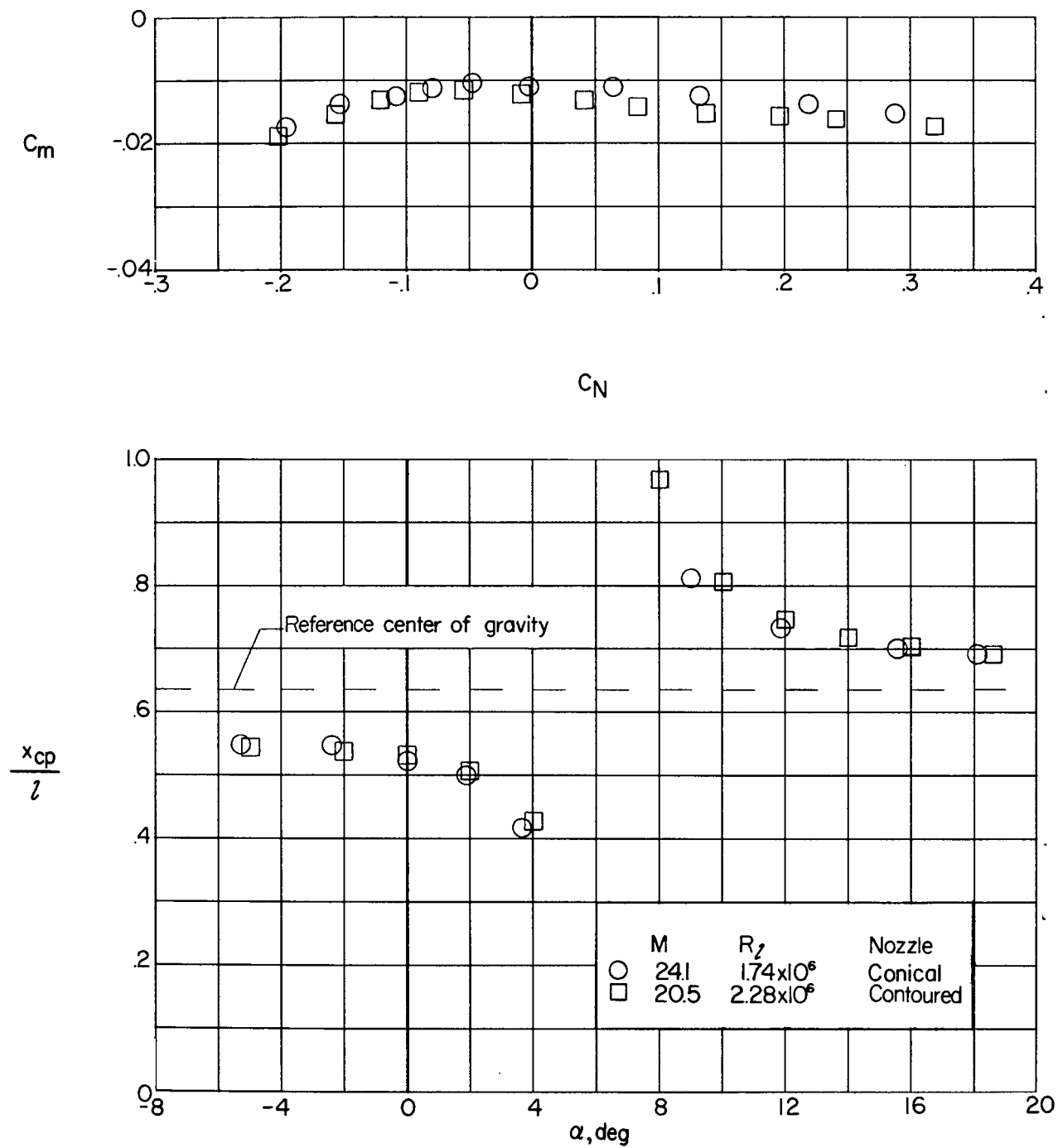


Figure 11.- Concluded.